AD-A146 304 COPLANAR SCHOTTKY VARIABLE PHASE SHIFTER(U) TEXAS UNIV AT AUSTIN DEPT OF ELECTRICAL ENGINEERING Y FUKUOKA ET AL. 13 AUG 84 UT-MW-N-84-6 1/1

UNCLASSIFIED N00014-79-C-0553 F/G 9/5 NL

END

FILMED

DTIC

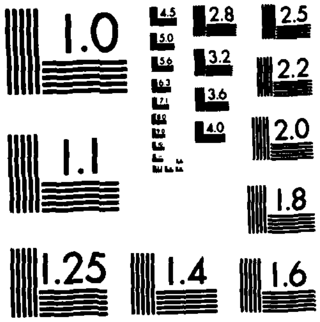

MICROCOPY RESOLUTION TEST CHART

AD-A146 304

(10)

MICROWAVE LABORATORY REPORT NO. 84-6

COPLANAR SCHOTTKY VARIABLE PHASE SHIFTER

by

Y. Fukuoka and T. Itoh

May 1984

SPONSORED BY THE OFFICE OF NAVAL RESEARCH

Contract No.: N00014-79-C-0553

DEPARTMENT OF ELECTRICAL ENGINEERING
THE UNIVERSITY OF TEXAS AT AUSTIN
AUSTIN, Texas 78712

SECURITY CLASSIFICATION OF THIS PAGE (When Data Entered)

REPORT DOCUMENTATION PAGE

READ INSTRUCTIONS BEFORE COMPLETING FORM

1. REPORT NUMBER UT-MW-N-84-6	2. GOVT ACCESSION NO. AD-A146304	3. RECIPIENT'S CATALOG NUMBER
4. TITLE (and Subtitle) Coplanar Schottky Variable Phase Shifter		5. TYPE OF REPORT & PERIOD COVERED Technical Report
		6. PERFORMING ORG. REPORT NUMBER
7. AUTHOR(s) Yoshiro Fukuoka and Tatsuo Itoh		8. CONTRACT OR GRANT NUMBER(s) N0014-79-C-0553
9. PERFORMING ORGANIZATION NAME AND ADDRESS University of Texas at Austin P.O. Box 7728 Austin, Texas 78712		10. PROGRAM ELEMENT, PROJECT, TASK AREA & WORK UNIT NUMBERS
11. CONTROLLING OFFICE NAME AND ADDRESS Office of Naval Research Arlington, VA 22217		12. REPORT DATE 8/13/84
		13. NUMBER OF PAGES 82
14. MONITORING AGENCY NAME & ADDRESS(if different from Controlling Office)		15. SECURITY CLASS. (of this report) Unclassifield
		15a. DECLASSIFICATION/DOWNGRADING SCHEDULE

16. DISTRIBUTION STATEMENT (of this Report)

Unlimited

17. DISTRIBUTION STATEMENT (of the abstract entered in Block 20, if different from Report)

18. SUPPLEMENTARY NOTES

19. KEY WORDS (Continue on reverse side if necessary and identify by block number)

PHASE SHIFTER, COPLANAR WAVEGUIDE, SLOW WAVE, SCHOTTKY CONTACT, MONOLITHIC INTEGRATED CIRCUIT

20. ABSTRACT (Continue on reverse side if necessary and identify by block number)

DD FORM 1 JAN 73 1473 EDITION OF 1 NOV 65 IS OBSOLETE
S/N 0102-014-6601

SECURITY CLASSIFICATION OF THIS PAGE (When Data Entered)

MICROWAVE LABORATORY REPORT NO. 84-6

COPLANAR SCHOTTKY VARIABLE PHASE SHIFTER

by

Y. Fukuoka and T. Itoh

May 1984

SPONSORED BY THE OFFICE OF NAVAL RESEARCH

Contract No.: N00014-79-C-0553

DEPARTMENT OF ELECTRICAL ENGINEERING
THE UNIVERSITY OF TEXAS AT AUSTIN
AUSTIN, Texas 78712

ABSTRACT

A coplanar Schottky variable phase shifter is studied. This device has a simple configuration and is suitable for monolithic integration. The device uses the electronic variability of the depletion layer thickness of the Schottky contact under the coplanar waveguide to change the amount of the phase shift. A periodic structure is introduced to reduce a loss caused by the existing semiconductor material which has a finite conductivity. An integral equation is formulated and solved by the point-matching method. The analysis allows one to predict the phase shift and the attenuation in the device. It is shown that such a device can operate at millimeter-wave frequencies with a very small loss. A simple measurement confirmed these predictions.

TABLE OF CONTENTS

Abstract i

List of Figures iii

List of Tables v

CHAPTER 1 : Introduction 1

CHAPTER 2 : Analysis of MIS Coplanar Waveguide 5

Method of Analysis 5

Computational Results 15

CHAPTER 3 : MIS Periodic Coplanar Waveguide 25

Approach 25

Results 28

CHAPTER 4 : Experiments 34

CHAPTER 5 : Coplanar Schottky Variable Phase Shifter 40

Conditions of Optimum Operation 42

Results 47

CHAPTER 6 : Conclusions 55

APPENDIX A : Derivation of the Integral Equation 56

APPENDIX B : Program Listing 68

References 80

LIST OF FIGURES

Figure 1 Schematic view of the coplanar waveguide constructed on the periodically doped, semiconductor substrate

Figure 2 Cross-sectional view of the analytical model of the MIS coplanar waveguide

Figure 3 Convergence of the solutions

Figure 4 (a) Slow-wave factor versus frequency (b) Attenuation constant versus frequency

Figure 5 Slow-wave factor versus frequency

Figure 6 Characteristic impedance of the MIS coplanar waveguide (a) Real part (b) Imaginary part

Figure 7 Two constituent sections of the MIS periodic coplanar waveguide

Figure 8 Comparison of the slow-wave factor of the MIS periodic coplanar waveguide with the uniform MIS coplanar waveguide

Figure 9 Comparison of the attenuation constant of the MIS periodic coplanar waveguide with the uniform MIS coplanar waveguide

Figure 10 Schematic view of the experimental model of the MIS periodic coplanar waveguide

Figure 11 Comparison between experiment and theory : (a) slow-wave factor (b) attenuation constant

Figure 12 (a) MIS coplanar waveguide (b) Schottky coplanar waveguide
Figure 13 Depletion layer thickness versus DC bias current for GaAs substrate
Figure 14 Behavior of the optimum conductivity
Figure 15 Behavior of the optimum conductivity
Figure 16 Attenuation constant versus conductivity of the doped region
Figure 17 (a) Required device length for various slot width (b) Total attenuation of the device
Figure 18 Total attenuation versus frequency

LIST OF TABLES

Table 1 Computed phase and attenuation constants obtained by several different methods

Table 2 Dimensions and material constants of the experimental models

Table 3 Various constants for GaAs substrate used in the calculation

CHAPTER 1 : INTRODUCTION

Transmission lines constructed on semiconductor substrate were first studied to investigate the behavior of the signal travelling in a semiconductor chip in a high speed computer. Several analyses based on parallel-plate models have been published, and it has been shown that such structures exhibit slow-wave characteristic under certain circumstances [1-3]. The electrical length of such a structure could be forty to fifty times longer than the physical length. This means that the effective dielectric constant could become one thousand or more. The waveguide structure usually contained two different media: an insulator and a doped semiconductor, which is often refered to as an MIS (metal-insu ator-semiconductor) structure. The slow-wave characteristic is caused by the phenomenon that the electric and magnetic energies are stored in different regions of the waveguide. The slow-wave phenomenon is interesting in microwave and millimeter-wave (mm-wave) applications such as delay lines and phase shifters. These transmission lines have either MIS configurations or Schottky-contacts on semiconductor substrates. In the latter case, the depletion layer formed under the Schottky-contact metal acts like an insulator region since it has a small conductivity compared to the surrounding doped semiconductor region. The propagation speed depends greatly on the thickness of the insulated layer under the metal. Therefore, the bias dependence of the Schottk-

y-contact depletion layer thickness can be used advantageously to construct an electronically variable phase shifter [4-6].

In practice, various planar structures can be used to realize the slow-wave structure, such as microstrip line and coplanar waveguide. Between these structures, a coplanar waveguide seems to be preferable for various applications because other devices can be connected in series or parallel. For this reason, this discussion is limited to the MIS and Schottky coplanar waveguide. These structures are also suitable for applications in monolithic microwave and millimeter-wave integrated circuits.

A large problem of these devices is, however, their inherently large attenuation caused by the finite conductivity of the semiconductor substrate. To obtain slow-wave propagatin up to a high frequency range, it is necessary to raise the conductivity of the semiconductor substrate to a large value, typically 10^4 to 10^5 S/m., which causes high attenuation at high frequencies. Not many investigators have tried to solve this problem. There were a few papers dealing with the reduction of the loss by replacing the semiconductor material by periodic metal strips [7-8]. The slow-wave propagation occuring in the structures is caused by the periodicity. Therefore, this structure only solves the attenuation problem for a fixed phase-delay line, and can not be applied to the Schottky-contact line with the property of the electronic variability of the depletion layer thickness.

In Part I of this dissertation, a new structure is presented to solve this problem: an MIS and Schottky periodic coplanar waveguide. As Fig. 1 shows, the proposed structure introduces periodic lossless sec-

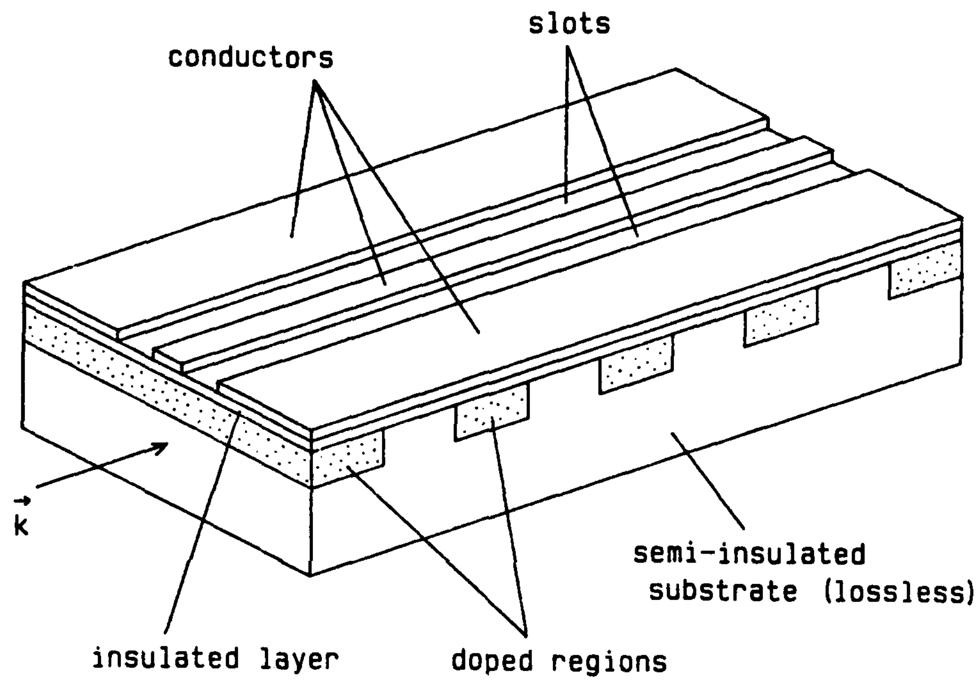

Figure 1 Schematic view of the coplanar waveguide constructed on the periodically doped semiconductor substrate

tions into the MIS or Schottky coplanar waveguide. In this way, the total attenuation of the device can be reduced since it has fewer lossy semiconductor regions. Also, the periodicity of the structure provides slow-wave propagation, and the total phase delay value can be improved.

Part I covers both theoretical and experimental study of such a structure. The theoretical analysis includes the MIS coplanar waveguide using an integral equation method and also the analysis of the periodic structure by conventional transmission line theory. The experiments were conducted performed to confirm the theory. Several models of the proposed structure were constructed, and tested at VHF and UHF frequencies. The results confirm the applicability of the theory. In the last chapter of Part I, optimum conditions for the operation of the coplanar Schottky variable phase shifter are discussed using the theoretical results. It will be shown that such a device can be used at mm-wave frequencies without the disadvantage of significant attenuation.

CHAPTER 2 : ANALYSIS OF MIS COPLANAR WAVEGUIDE

In this chapter, the propagation characteristics of the MIS coplanar waveguide are discussed. An elaborate method of analyzing this structure is developed which is capable of predicting the frequency dependence of the propagation characteristics. From the result of this analysis, the frequency region of the slow-wave propagation, the value of the slow-wave factor, the attenuation constant, and the characteristic impedance can be determined. Since the MIS coplanar waveguide is a special case of the MIS periodic coplanar waveguide, the results of this analytical method are used in the following chapters to determine the characteristics of the periodic structure as well.

METHOD OF ANALYSIS

Several previous studies have shown the applicability of diverse techniques to the analysis of MIS coplanar waveguide. The spectral-domain method, mode-matching method, and finite element method have all been used [9-15]. The convergence of the solutions in these methods is dependent on the actual field distribution in the MIS coplanar waveguide and the choice of basis functions in the analysis. In the MIS coplanar waveguide, the field around the slot region is deformed by the highly conductive doped region located near the coductors. Therefore,

the spatial gradients of the field components are large near the edges of the conductors, and hence, many basis functions are needed in that region to express them [15].

Yamashita introduced a hybrid-mode analysis technique to solve lossless planar structures with various configurations [16]. In his technique, an integral equation is first constructed with respect to unknown field components, and is then solved by non-uniform discretization. Matching points are taken so that more points are located near the edges of the conductors to make the convergence of the solutions faster. This technique is especially well suited for the structure under consideration, because larger spatial gradients of the field components near the edges of the conductors are expected compared to the conventional lossless structures. Another advantage of this technique is that it can easily be used to calculate the characteristic impedance of the structure by choosing appropriate field components as the unknown functions of the integral equation. Also, this method is a full-wave analysis, and is used to obtain the frequency dependence of the characteriscs. This is important since the slow-wave phenomenon of the MIS structure strongly depends on frequency.

For convenience, the cross section of the MIS coplanar waveguide is modeled as in Fig. 2. The substrate is divided into three layers each of uniform thickness: the insulated layer, the doped layer, and the semi-insulated layer (Regions 2, 3, and 4 in the figure, respectively). These regions are assumed to be linear, homogeneous, and isotropic. That is, material properties are uniform in each region, and are characterized by a single dielectric constant and conductivity.

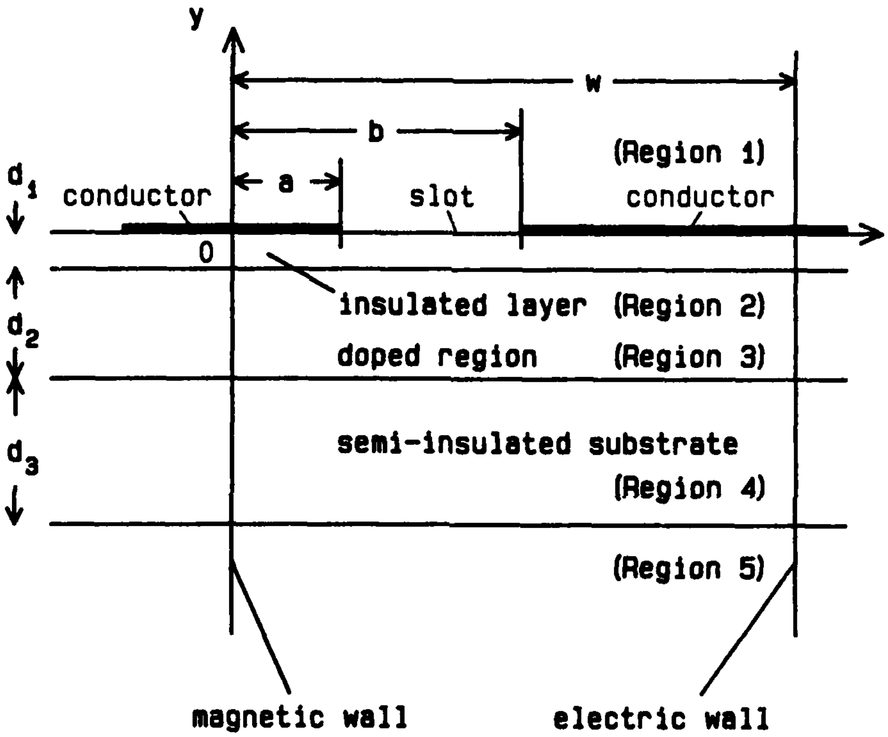

Figure 2 Cross-sectional view of the analytical model of the MIS coplanar waveguide

The conductivity of the material is included in the imaginary part of the dielectric constant. The metal layer is assumed to be infinitesimally thin and to be perfectly conductive. Because the structure is symmetric and we are interested only in the dominant mode, which has even symmetry, we can place a vertical magnetic wall at the center (x=0) and consider only the right half of the structure. The tangential components of the magnetic field vanish at the magnetic wall. An electric wall (perfect conductor) is then placed at the far right (x=w, w>>b) for analytical convenience. This way, we can generate a discrete Fourier series solution.

The analysis is based on the electric and magnetic vector potentials, $\vec{F}$ and $\vec{A}$, respectively [17]. These potentials satisfy the following equations:

$$\nabla \times \nabla \times \vec{A} - k^2\vec{A} = - \frac{1}{j\omega\varepsilon} \nabla \Phi_a \tag{1}$$

$$\nabla \times \nabla \times \vec{F} - k^2\vec{F} = - \frac{1}{j\omega\mu} \nabla \Phi_f \tag{2}$$

where k is the complex wave number, ω is angular frequency, ε is the complex dielectric permittivity, μ is the magnetic permeability, and Φ_a and Φ_f are arbitrary scalar functions. In our case, it is convenient to choose

$$\vec{A} = \psi \vec{y} \tag{3}$$

$$\vec{F} = \phi \vec{y} \tag{4}$$

where ψ and ϕ are the scalar functions which represent the wave transverse electric (TE) wave and transverse magnetic wave (TM) to the y-direction, respectively, and $\vec{y}$ is a unit vector in the y-direction. The electric and magnetic field vectors can be derived from these quantities:

$$\vec{E} = - \nabla \times \vec{F} + \frac{1}{j\omega\varepsilon} \nabla \times \nabla \times \vec{A} \tag{5}$$

$$\vec{H} = \nabla \times \vec{A} + \frac{1}{j\omega\mu} \nabla \times \nabla \times \vec{F} \tag{6}$$

where $\vec{E}$ and $\vec{H}$ are the electric and magnetic field vectors, respectively. These potentials are expanded in terms of their eigenfunctions, which should be either sinusoidal or exponential functions and must satisfy the boundary conditions on the vertical magnetic and electric walls. The potentials in each region can be expressed as follows:

$$\psi_1 = \sum_n A_n \cos\beta_n x \, e^{-\alpha_{1n} y}$$

$$\phi_1 = \sum_n B_n \sin\beta_n x \, e^{-\alpha_{1n} y}$$

(Region 1) (7)

$$\psi_2 = \sum_n \cos\beta_n x \, (C_n \sin\alpha_{2n} y + C'_n \cos\alpha_{2n} y)$$

$$\phi_2 = \sum_n \sin\beta_n x \, (D_n \sin\alpha_{2n} y + D'_n \cos\alpha_{2n} y)$$

(Region 2) (8)

$$\psi_3 = \sum_n \cos\beta_n x \, [E_n \sin\alpha_{3n}(y+d_1) + E'_n \cos\alpha_{3n}(y+d_1)]$$

$$\phi_3 = \sum_n \sin\beta_n x \, [F_n \sin\alpha_{3n}(y+d_1) + F'_n \cos\alpha_{3n}(y+d_1)]$$

(Region 3) (9)

$$\psi_4 = \sum_n \cos\beta_n x \, [G_n \sin\alpha_{4n}(y+d_1+d_2) + G'_n \cos\alpha_{4n}(y+d_1+d_2)]$$

$$\phi_4 = \sum_n \sin\beta_n x \, [H_n \sin\alpha_{4n}(y+d_1+d_2) + H'_n \cos\alpha_{4n}(y+d_1+d_2)]$$

(Region 4) (10)

$$\phi_5 = \sum_n I_n \cos\beta_n x \; e^{\alpha_{5n}(y+d_1+d_2+d_3)}$$

$$\phi_5 = \sum_n J_n \sin\beta_n x \; e^{\alpha_{5n}(y+d_1+d_2+d_3)}$$

(Region 5) (11)

The z-dependence is omitted from each of the above expressions and assumed to be of the form:

$$e^{-j\gamma z}$$

where γ is the propagation constant in the z-direction and:

$$\beta_n = \left(n - \frac{1}{2} \right) \frac{\pi}{w}$$

$$\alpha_{in}^2 = \gamma^2 + \beta_n^2 + \omega^2 \varepsilon_2 \mu_o$$

The summations over n range from one to infinity, and A_n, B_n, etc. are constants to be calculated from the boundary conditions. The potentials in Regions 1 and 5 are chosen so that the field decays exponentially as y approaches $\pm\infty$ in each region.

The coefficients of the potentials are adjusted to satisfy the boundary conditions at $y=-d_1$, $-(d_1+d_2)$, and $-(d_1+d_2+d_3)$. These are easily adjusted by comparing the coefficients of the terms of the same value

of n in the summation in separate expressions, since the associate eigenfunctions have the same variation in the x-direction. Doing this eliminates a number of the unknown coefficients, and the potentials in the insulated region (Region 2) can then be written as

$$\psi_2 = - \sum_n \frac{\varepsilon_2 \alpha_{1n}}{\varepsilon_1 \alpha_{2n}} A_n \cos\beta_n x \, (\sin\alpha_{2n} y + P_{cn} \cos\alpha_{2n} y)$$

$$\phi_2 = \sum_n B_n \sin\beta_n x \, (P_{dn} \sin\alpha_{2n} y + \cos\alpha_{2n} y) \qquad (12)$$

P_{cn} and P_{dn} are the constants determined by this process. Derivation of these values is explained in Appendix A.

The x and z components of the electric field are required to be continuous at the plane where conductors are placed (y=0) and to be zero on the conductors (y=0 and 0<x<a, b<x<w), and the x and z components of the magnetic field to be continuous in the slot region (y=0 and a<x<b). This process is summarized as follows:

At y=0,

$E_{x1} = E_{x2}$	0<x<w
$E_{z1} = E_{z2}$	0<x<w
$E_{x1} = 0$	0<x<a, b<x<w
$E_{z1} = 0$	0<x<a, b<x<w
$H_{x1} - H_{x2} = 0$	a<x<b
$H_{z1} - H_{z2} = 0$	a<x<b

(13)

After satisfying these conditions, standard Fourier analysis is used to derive the integral equation:

$$\sum_n \left[P_n \int_s f(x') \sin\beta_n x' \, dx' + Q_n \int_c g(x') \cos\beta_n x' \, dx' \right] \cos\beta_n x = 0$$

$$0<x<a, \quad b<x<w$$

$$\sum_n \left[R_n \int_s f(x') \sin\beta_n x' \, dx' + P_n \int_c g(x') \cos\beta_n x' \, dx' \right] \sin\beta_n x = 0$$

$$a<x<b$$

(14)

where labels s and c represent the integration range over the slot and conductors, respectively. *f(x) is proportional to the x component of the* electric field in the slot region and g(x) is proportional to the current density on the conductors:

$$f(x) \propto E_{x1} \qquad a<x<b$$

$$g(x) \propto H_{x1} - H_{x2} \qquad 0<x<a, \quad b<x<w$$

(15)

The expressions of the coefficients P_n, Q_n, and R_n are also given in Appendix A. The main reason to choose E_x and J_z as unknown functions in the integral equations is that it will be easy to calculate the characteristic impedance of the structure after we obtain the solution.

The integral equation (14) is solved by the point matching method. Matching points are selected non-uniformly along the y=0 plane to make the convergence of the solution faster. More points are selected near the edges of the conductors to accommodate the gradients in the field components. The unknown functions E_x and J_z are assumed to be constant between two adjacent matching points. Then a system of linear equations can be obtained. This is written in matrix form:

$$Z\,u = 0 \tag{16}$$

where Z is a two-dimensional matrix with the size of $N_p \times N_p$, where N_p is the number of the matching points, and a column vector u contains unknown function values f(x) and g(x) between matching points. A nontrivial solution is obtained only if the matrix Z is singular. Therefore, we seek this condition by varying the value of the propagation constant. This is a complex value since the equation is complex. Both phase and attenuation constants can be obtained from its real and imaginary parts.

The characteristic impedance is calculated as follows. After the complex propagation constant is obtained, the unknown functions f(x) and g(x) can be calculated to obtain approximate values of E_x and J_z. The characteristic impedance is then given by:

$$Z_c = \frac{\int_a^b E_x(x)\,dx}{2\int_0^a J_z(x)\,dx} \tag{17}$$

The numerator of equation (17) represents the voltage across the slot region and the denominator represents the total current flowing on the center conductor into the z direction.

COMPUTATIONAL RESULTS

According to the above theory, a FORTRAN program was written and the integral equation (14) was successfully solved. A CDC Dual Cyber 170/370 at The University of Texas Computation Center was used for all calculations. The evaluation of the singularity of the matrix **Z** was done by looking at the numerically calculated values of the determinant and the condition number of the matrix. These values were obtained by the Gaussian elimination method using the LINPACK subroutines in The University of Texas numerical analysis libraries. The accuracy of the singularity obtained for the matrix was checked using the singular-value decomposition method which is also in the LINPACK subroutines. The search for the complex propagation constant was done by using the complex root-search routine ZANLYT in the IMSL subroutines, which uses the Muller's method with deflation. A solution was usually obtained in very small number of iterations, typically 6 to 10 times depending on the

starting point of the iteration. The summations in the integral equation (14) have complicated forms and therefore need to be truncated. To check the accuracy, the behavior of the results with respect to the number of terms in the summations over n and the number of matching points was investigated. It is not easy to investigate either of these analytically, since both of them strongly depend on the dimensions of the structure. Therefore, the convergence of the solutions was checked numerically. An example of the convergence studies is shown in Fig. 3, which is calculated for a typical MIS coplanar waveguide. The figure shows errors relative to the values at $N_p=30$. For a fixed value of N_p, the convergence of the solutions is tested with respect to the number of terms in the summations, and the converged values are plotted in the figure. The curves are not very smooth. This is caused by the nonuniformity in the distribution of the matching points. For fixed values of material constants, such as dielectric constants and conductivities, the convergence is faster if the thickness of the insulated layer (Region 2) is larger. Thinner insulated layers cause the fields to abruptly change near the edges of the conductors, therefore it requires more matching points and more terms in the summations to fit them. If there is no doped semiconductor layer (a conventional lossless coplanar waveguide), then the fields change very smoothly. Therefore, it requires fewer matching points and fewer terms in the summations to obtain precise solutions.

Computed frequency characteristics of the slow-wave factor, λ_o/λ_g, (λ_o is the wavelength in free space and λ_g is the wavelength in the guide) and the attenuation constant of the MIS coplanar waveguide is

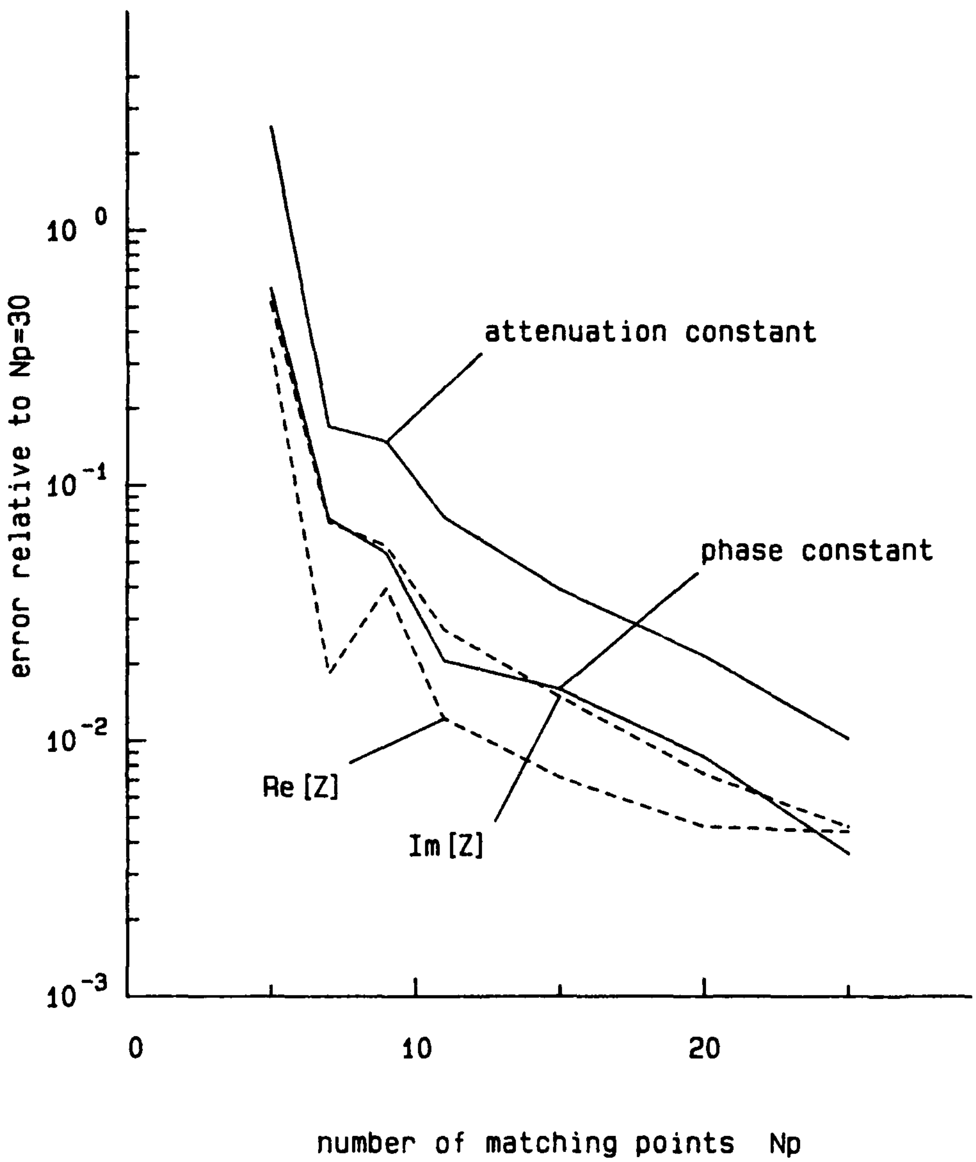

Figure 3 Convergence of the solutions

a=0.05mm, b=0.5mm, d_1=1.0μm, d_2=3.0μm

d_3=1.0mm, $\varepsilon_2=8.5\varepsilon_0$, $\varepsilon_3=\varepsilon_4=13.0\varepsilon_0$

$\sigma_3=10^4$S/m, f=100MHz

shown in Fig. 4. Experimental values obtained by Hasegawa are also shown for comparison [10]. They are in reasonably good agreement. As the figure shows, slow-wave propagation exists in the low frequency range, and becomes less pronounced as the frequency increases. The transition frequency is dependent on the value of the conductivity of the doped region. This dependence is shown in Fig. 5. There exists an optimum conductivity at which the transition frequency of the slow-wave region extends to the largest value [12]. This is important for the mm-wave operation of the device.

The numerical values of the phase and attenuation constants are also shown in Table 1 along with the values obtained by some other methods for comparison [15]. They agree well one another, which proves the precision of the proposed method. The frequency dependence of the characteristic impedance is shown in the next figure (Fig. 6). The values of the characteristic impedances agree with those obtained by Wen using a quasi-TEM result for the lossless case [18]. The different tendencies of the two curves in Fig. 6 will be discussed in Chapter 3 in conjunction with the results obtained for the MIS periodic coplanar waveguide.

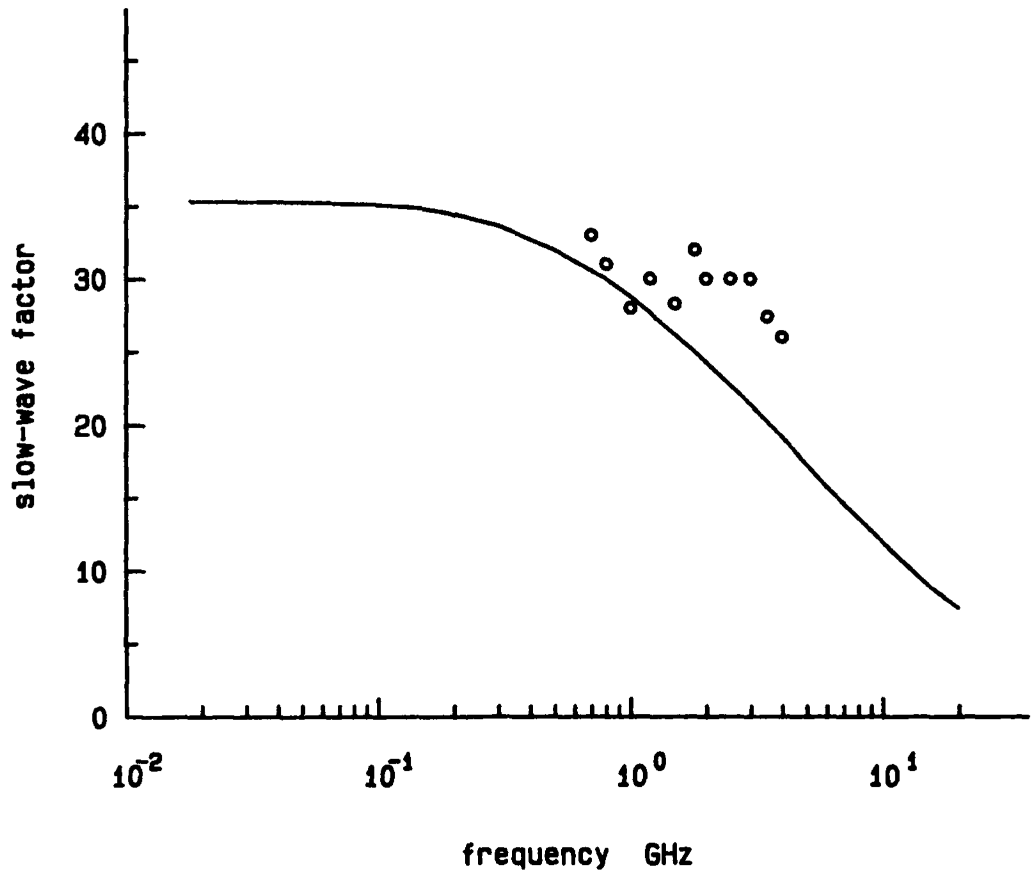

Figure 4a Slow-wave factor versus frequency

o : experiment [10]

a=0.05mm, b=0.5mm, d_1=0.4μm, d_2=3.0μm,

d_3=1.0mm, $\varepsilon_2=8.5\varepsilon_0$, $\varepsilon_3=\varepsilon_4=13.0\varepsilon_0$,

$\sigma_3=1.82\times10^4$S/m

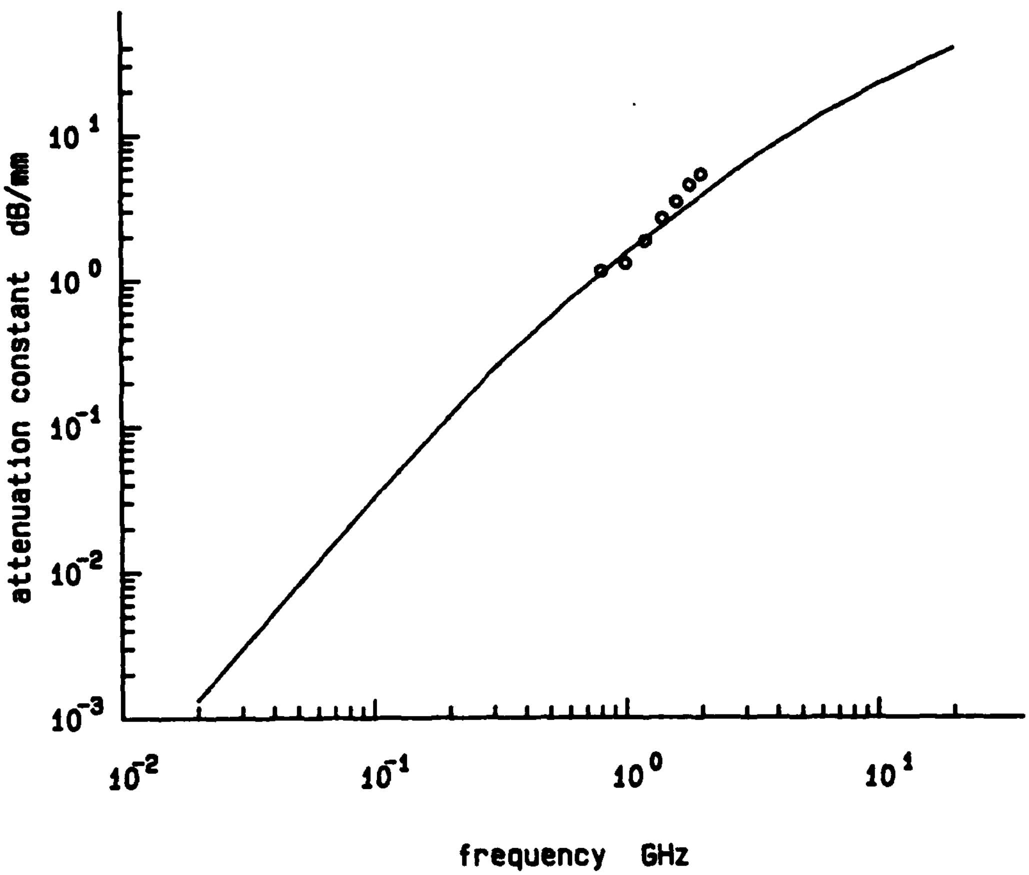

Figure 4b Attenuation constant versus frequency

o : experiment [8]

$a=0.05mm$, $b=0.5mm$, $d_1=0.4\mu m$, $d_2=3.0\mu m$,

$d_3=1.0mm$, $\varepsilon_2=8.5\varepsilon_0$, $\varepsilon_3=\varepsilon_4=13.0\varepsilon_0$,

$\sigma_3=1.82\times10^4 S/m$

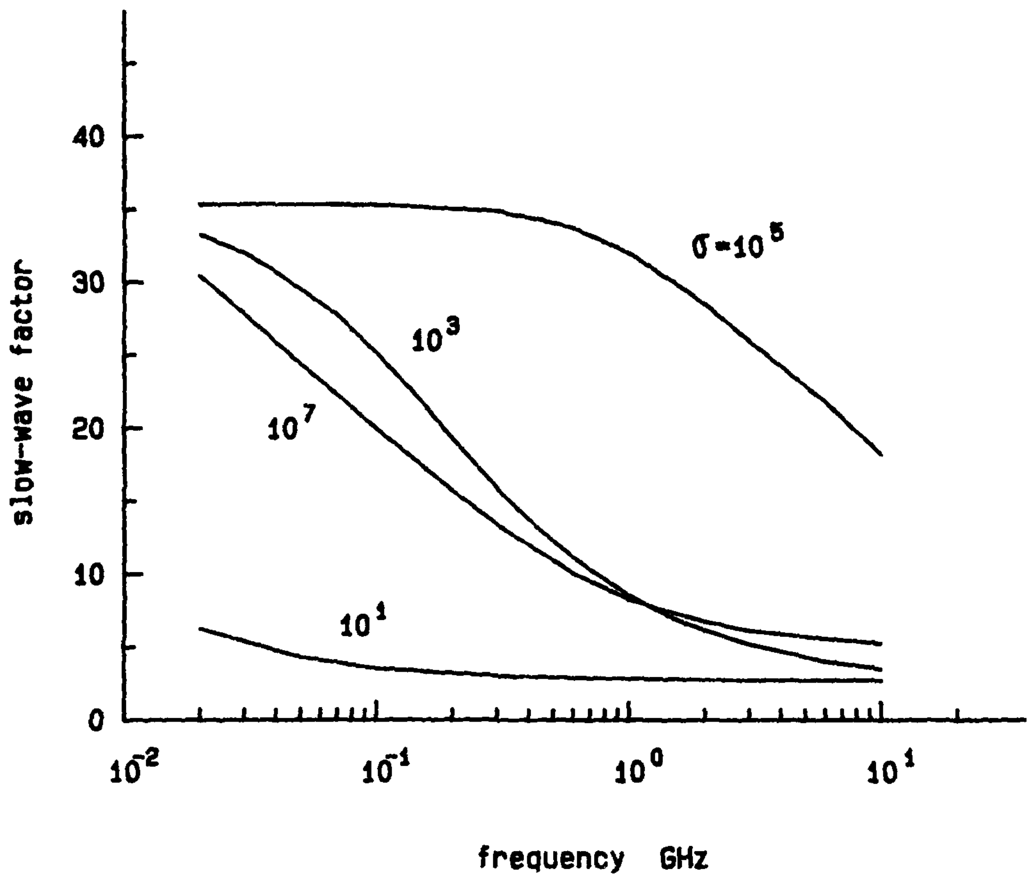

Figure 5 Slow-wave factor versus frequency : There exists an optimum conductivity σ to give a maximum slow-wave range.

$a=0.05mm$, $b=0.5mm$, $d_1=0.4\mu m$, $d_2=3.0\mu m$, $d_3=1.0mm$, $\varepsilon_2=8.5\varepsilon_0$, $\varepsilon_3=\varepsilon_4=13.0\varepsilon_0$

Table 1 Computed phase and attenuation constants obtained by several different methods

	Spectral-domain	Mode-matching	Present method
$f = 0.1$ GHz			
β/k_o	37.91	35.67	35.10
α	0.0466	0.0386	0.0322
$f = 1.0$ GHz			
β/k_o	31.61	29.87	28.81
α	1.76	1.56	1.51

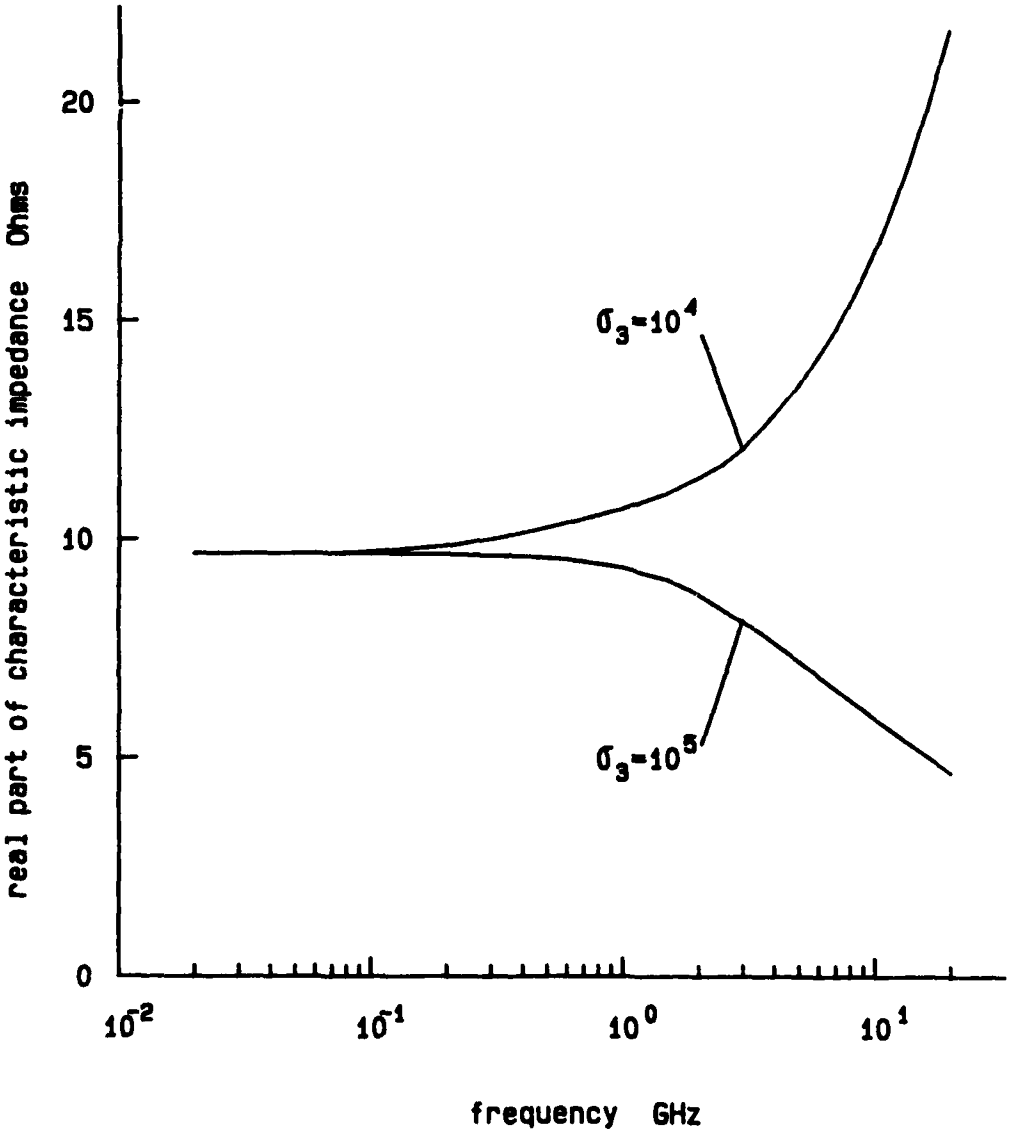

Figure 6a Real part of the characteristic impedance of the MIS coplanar waveguide
$a=0.05mm$, $b=0.5mm$, $d_1=1.0\mu m$, $d_2=3.0\mu m$,
$d_3=1.0mm$, $\varepsilon_2=8.5\varepsilon_o$, $\varepsilon_3=\varepsilon_4=13.0\varepsilon_o$,
$\sigma_3=10^4 S/m$

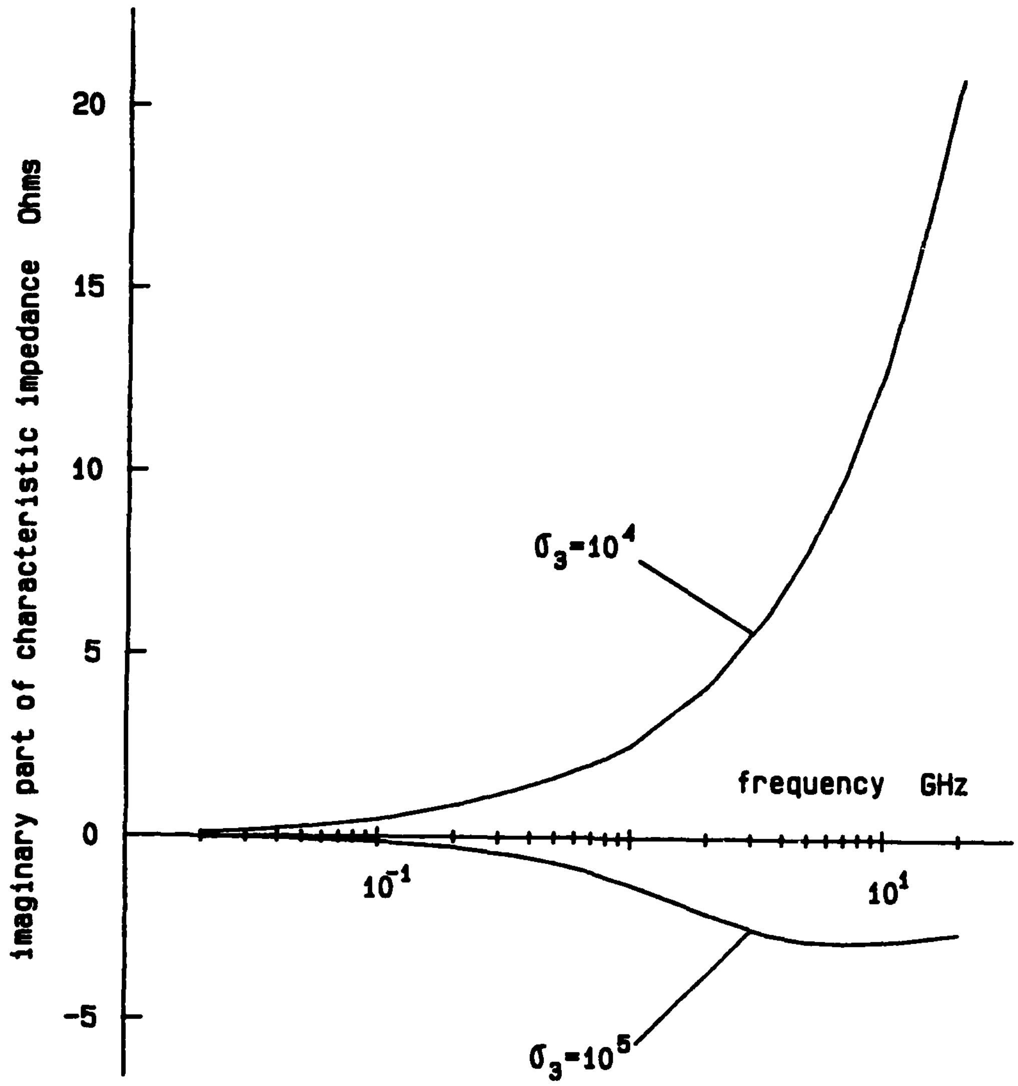

Figure 6b Imaginary part of the characteristic impedance of the MIS coplanar waveguide
$a=0.05$mm, $b=0.5$mm, $d_1=1.0\mu$m, $d_2=3.0\mu$m, $d_3=1.0$mm, $\varepsilon_2=8.5\varepsilon_0$, $\varepsilon_3=\varepsilon_4=13.0\varepsilon_0$, $\sigma_3=10^4$S/m

CHAPTER 3 : MIS PERIODIC COPLANAR WAVEGUIDE

As shown in the previous chapter, the MIS coplanar waveguide has a very large slow-wave factor below a certain critical frequency. For example, the result shown in the Fig. 4 indicates that the electrical length of the device at 1 GHz is about 30 times larger than the physical device length. However, high attenuation may make the application of such structures difficult.

In this chapter, a periodic structure is introduced to reduce this attenuation. The calculated result shows that the MIS periodic coplanar waveguide has advantages over the uniform structure.

APPROACH

The basic theoretical treatment of the MIS periodic coplanar waveguide consists of using Floquet's theorem for periodic transmission lines. To do this, reasonably accurate values of both propagation constant and characteristic impedance of the constituent sections of each period need to be calculated. Using the numerical method developed in the previous chapter, these values can be calculated and the MIS periodic coplanar waveguide can be analyzed (Fig. 1). The periodic structure consists of two different sections: one is an MIS coplanar waveguide and the other a lossless coplanar waveguide on the substrate with two differ-

ent materials (insulated layer and semi-insulated semiconductor substrate). Therefore, the easiest way to analyze this structure is to treat it as a periodic transmission line consisting of two lines with different characteristics; each line is characterized by its characteristic impedance and electrical length (Fig. 7). In this approach, the effect of the geometrical discontinuity at the junction of two sections is neglected, which is, however, assumed to be small.

The overall propagation characteristic of the MIS periodic coplanar waveguide is approximately calculated by applying Floquet's theorem [19]:

$$\cos\theta = \cos\theta_1 \cos\theta_2 - \frac{1}{2}\left[\frac{Z_1}{Z_2} + \frac{Z_2}{Z_1}\right] \sin\theta_1 \sin\theta_2 \tag{18}$$

where

$\theta = \gamma \ell, \quad \theta_1 = \gamma_1 \ell_1, \quad \theta_2 = \gamma_2 \ell_2$

$\ell = \ell_1 + \ell_2 \quad : \quad \ell_1, \ell_2$ length of eacy section

The characteristic impedances (Z_1, Z_2) and the propagation constants (γ_1, γ_2) of two sections are calculated by applying the numerical method discussed. The propagation constant (γ) of the periodic structure obtained by solving eq. (18) is again a complex value, from which we can investigate the attenuation constant and the slow-wave factor.

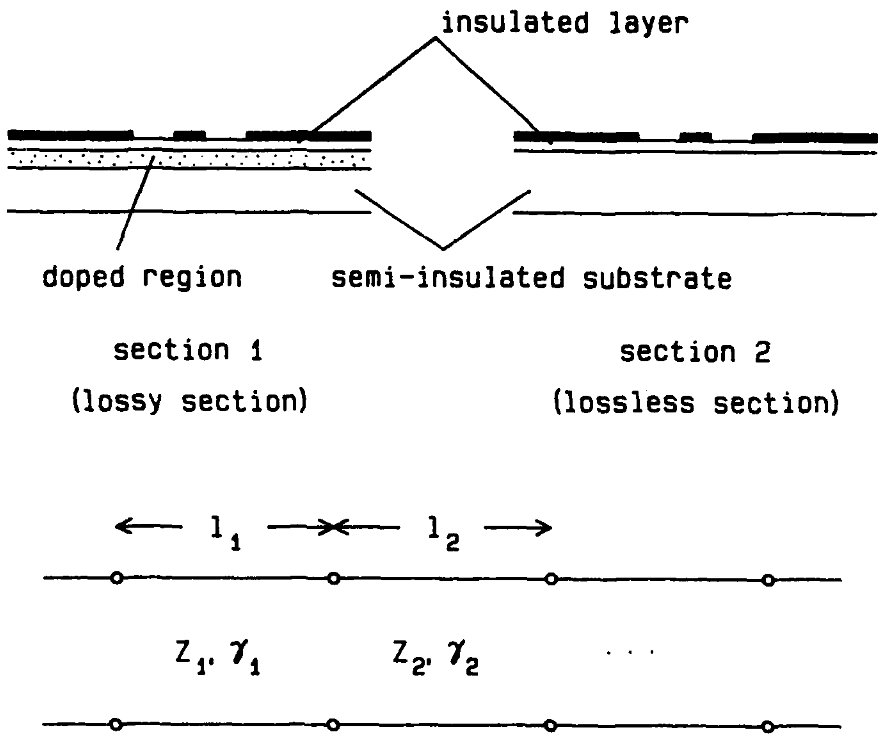

Figure 7 Two constituent sections of the MIS periodic coplanar waveguide : Each section is characterized by its electrical length and the characteristic impedance.

RESULTS

The computed slow-wave factors and attenuation constants for MIS periodic coplanar waveguide are presented in Fig. 8 and Fig. 9, respectively. Two typical cases are shown in the figures. A remarkable result is obtained for the case $\sigma_3=10^5$ S/m (Fig. 8a), where the extension of the frequency range of the slow-wave propagation is observed. Namely, the slow-wave factor of the periodic structure becomes greater than that of uniform MIS coplanar waveguide at frequencies higher than 10 GHz. This crossover of the slow-wave factor occurs for conductivities larger than a certain critical value. For instance, no crossover point exists for $\sigma_3=10^4$ S/m (Fig. 8b). This difference can be explained by the behavior of the doped layer. A highly conductive doped layer tends to act like a conductor at high frequencies [2]. This tendency can also be seen from the results of the previous chapter, Fig. 6, where the real part of the characteristic impedance of the MIS coplanar waveguide becomes smaller at high frequencies for $\sigma_3=10^5$ S/m. Therefore the effect of periodicity becomes strong and provides slow-wave propagation in this frequency range. In fact, if the doped regions of the MIS periodic coplanar waveguide are replaced by conductor strips, the resulting slow-wave factor follows nearly the same curve at high frequencies. On the other hand, a doped layer with low conductivity acts as a dielectric layer, and the periodicity becomes weak at high frequencies. Therefore the real part of the characteristic impedance of the MIS coplanar waveguide becomes larger at high frequencies (Fig. 6a). In this case, the periodic structure does not provide the enhancement to the slow-wave

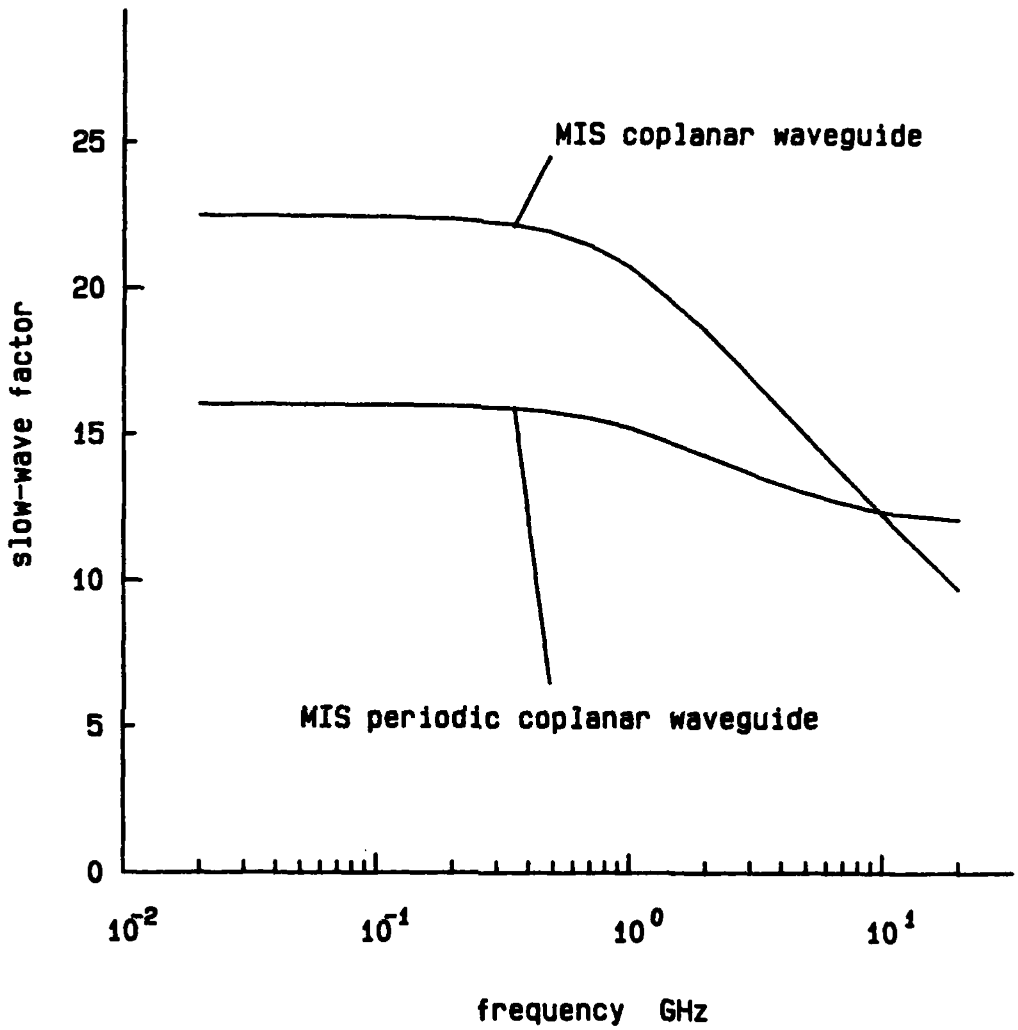

Figure 8a Comparison of the slow-wave factor of the MIS periodic coplanar waveguide with the uniform MIS coplanar waveguide

$a=0.05$mm, $b=0.5$mm, $d_1=1.0\mu$m, $d_2=3.0\mu$m, $d_3=1.0$mm, $\varepsilon_2=8.5\varepsilon_0$, $\varepsilon_3=\varepsilon_4=13.0\varepsilon_0$, $\sigma_3=10^5$S/m, $\ell_1=\ell_2=0.1$mm

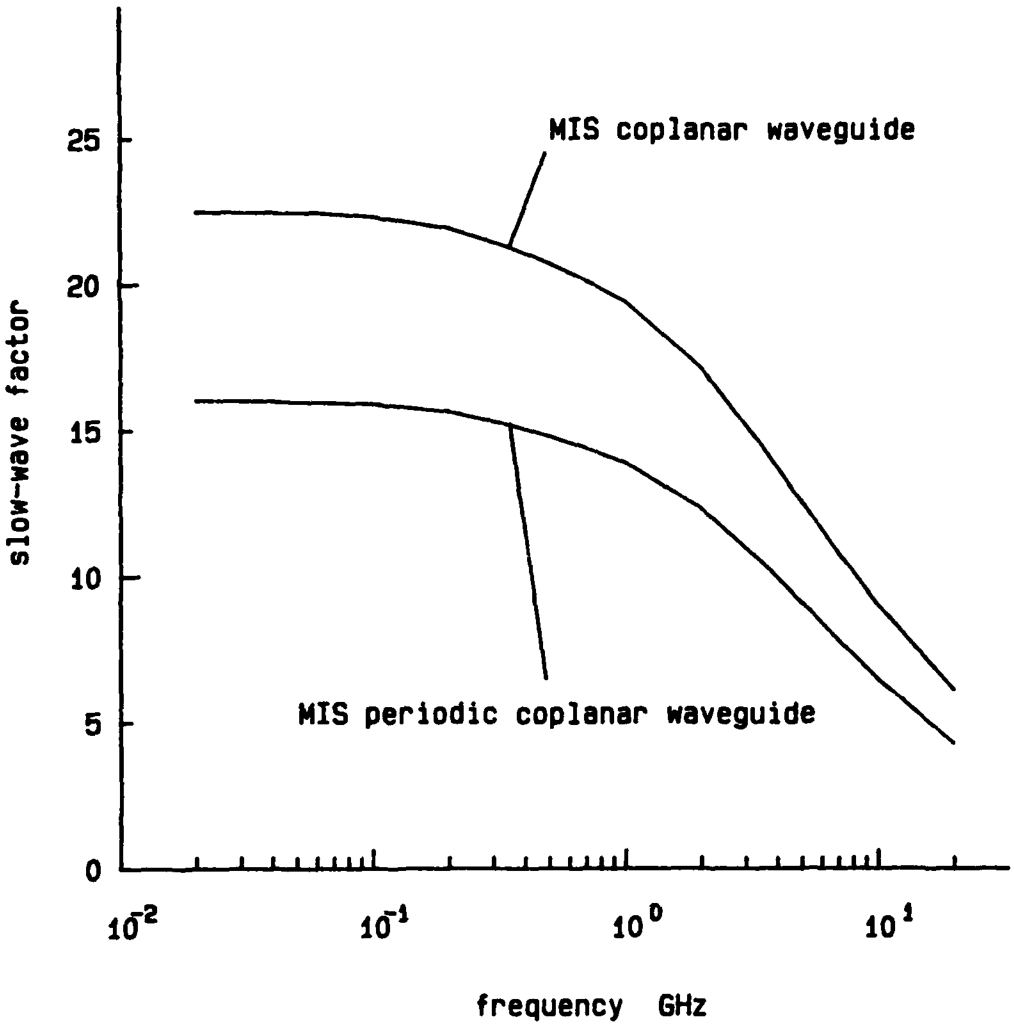

Figure 8b Comparison of the slow-wave factor of the MIS periodic coplanar waveguide with the uniform MIS coplanar waveguide

$a=0.05mm$, $b=0.5mm$, $d_1=1.0\mu m$, $d_2=3.0\mu m$,

$d_3=1.0mm$, $\varepsilon_2=8.5\varepsilon_0$, $\varepsilon_3=\varepsilon_4=13.0\varepsilon_0$,

$\sigma_3=10^4 S/m$, $\ell_1=\ell_2=0.1mm$

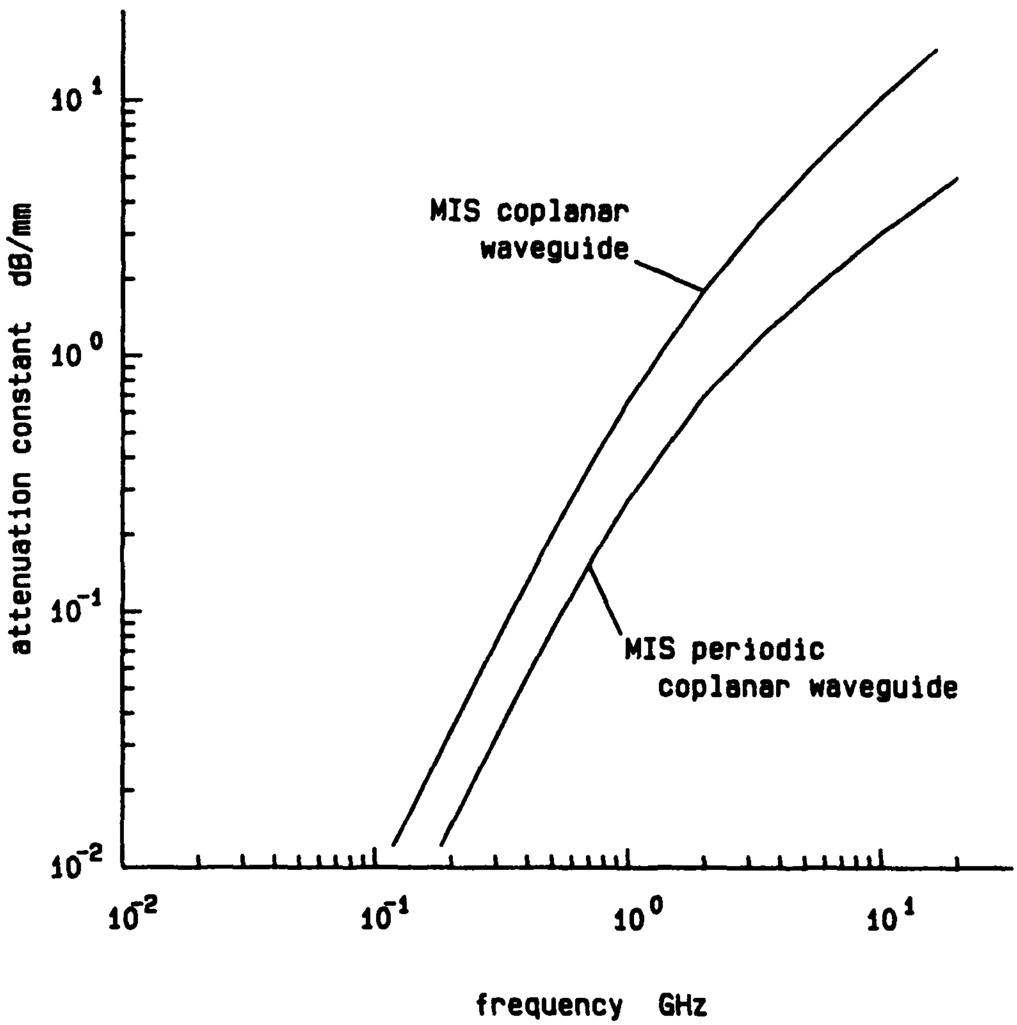

Figure 9a Comparison of the attenuation constant of the MIS periodic coplanar waveguide with the uniform MIS coplanar waveguide

$a=0.05$mm, $b=0.5$mm, $d_1=1.0\mu$m, $d_2=3.0\mu$m, $d_3=1.0$mm, $\varepsilon_2=8.5\varepsilon_0$, $\varepsilon_3=\varepsilon_4=13.0\varepsilon_0$, $\sigma_3=10^5$S/m, $\ell_1=\ell_2=0.1$mm

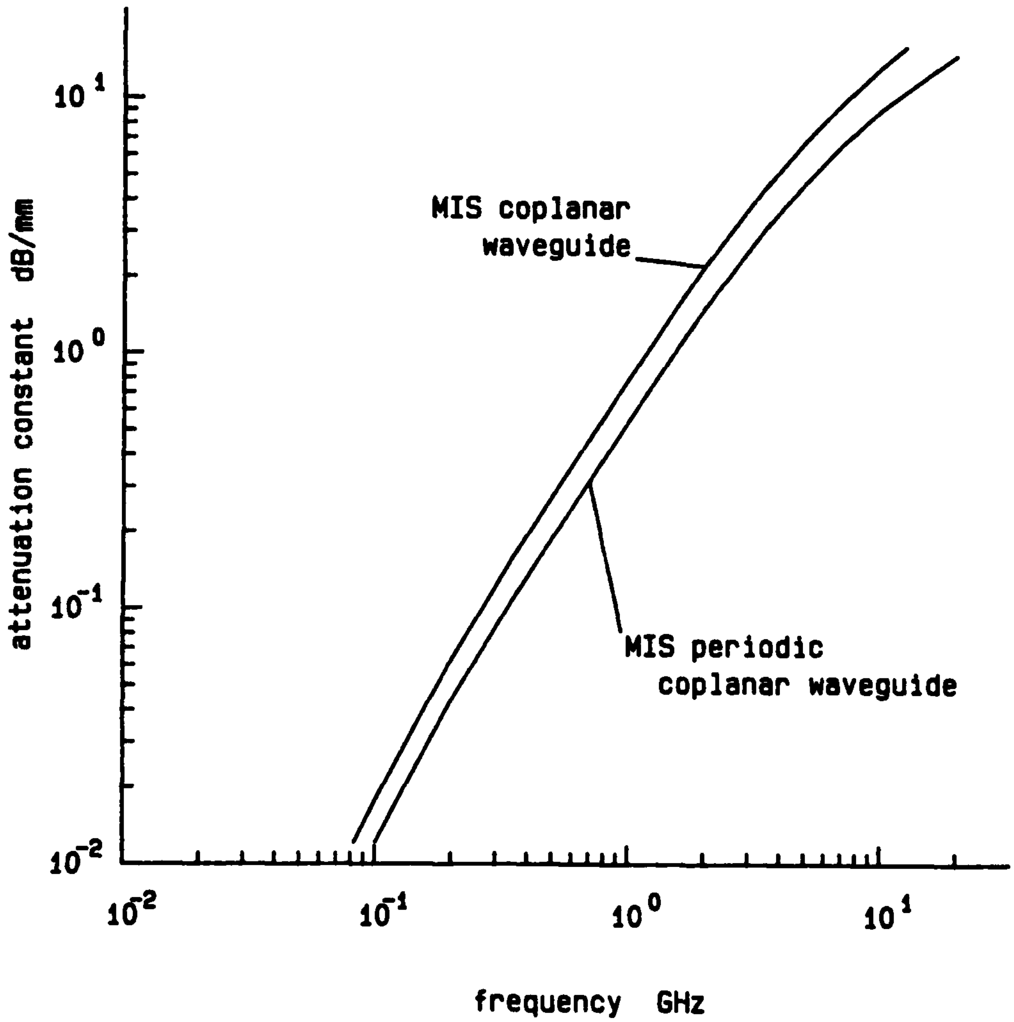

Figure 9b Comparison of the attenuation constant of the MIS periodic coplanar waveguide with the uniform MIS coplanar waveguide

a=0.05mm, b=0.5mm, d_1=1.0μm, d_2=3.0μm, d_3=1.0mm, $\varepsilon_2=8.5\varepsilon_o$, $\varepsilon_3=\varepsilon_4=13.0\varepsilon_o$, $\sigma_3=10^4$S/m, $\ell_1=\ell_2$=0.1mm

behavior. The reduction of attenuation constant is also more pronounced for the case $\sigma_3=10^5$ S/m compared to the other case (Fig. 9). Therefore, the MIS periodic coplanar waveguide is useful when the conductivity of the doped regions is larger than a certain critical value around 10^5 S/m, which corresponds to the doping level of around 10^{24} /m^3 in gallium arsenide (GaAs) substrate. This point will also be discussed in Chapter 5.

CHAPTER 4 : EXPERIMENTS

To justify our theory, a simple model of the MIS periodic coplanar waveguide was fabricated and tested in the frequency range of 40 MHz to 1 GHz. Complex propagation constants were measured using a conventional impedance measurement setup. Instead of a doped semiconductor substrate, graphite powder was used as a conductive material. The graphite powder was carefully sandwiched by two adhesive plastic sheets, and placed periodically on the coplanar waveguide etched on a circuit board, which has approximately the same dielectric constant as the plastic sheets (Fig. 10). A model of the uniform MIS coplanar waveguide is also fabricated using the same materials. The dimensions and other parameters of these two models are shown in Table 2.

The input impedances of the fabricated lines with open and short terminations were measured using an admittance bridge and the results were converted into the slow-wave factors and attenuation constants. The conductivity of the graphite layer, estimated from the measured results of the propagation constants of the model of the uniform MIS coplanar waveguide, was about 20 S/m. The nominal dielectric constant of the graphite layer was assumed to be unity since the graphite is a conductive material. The experimental results are shown in Fig. 11. Since we used the graphite powder to create conductive layers in the coplanar waveguide, they were not quite uniform in thickness and density. Nevertheless, the experimental results are in reasonably good

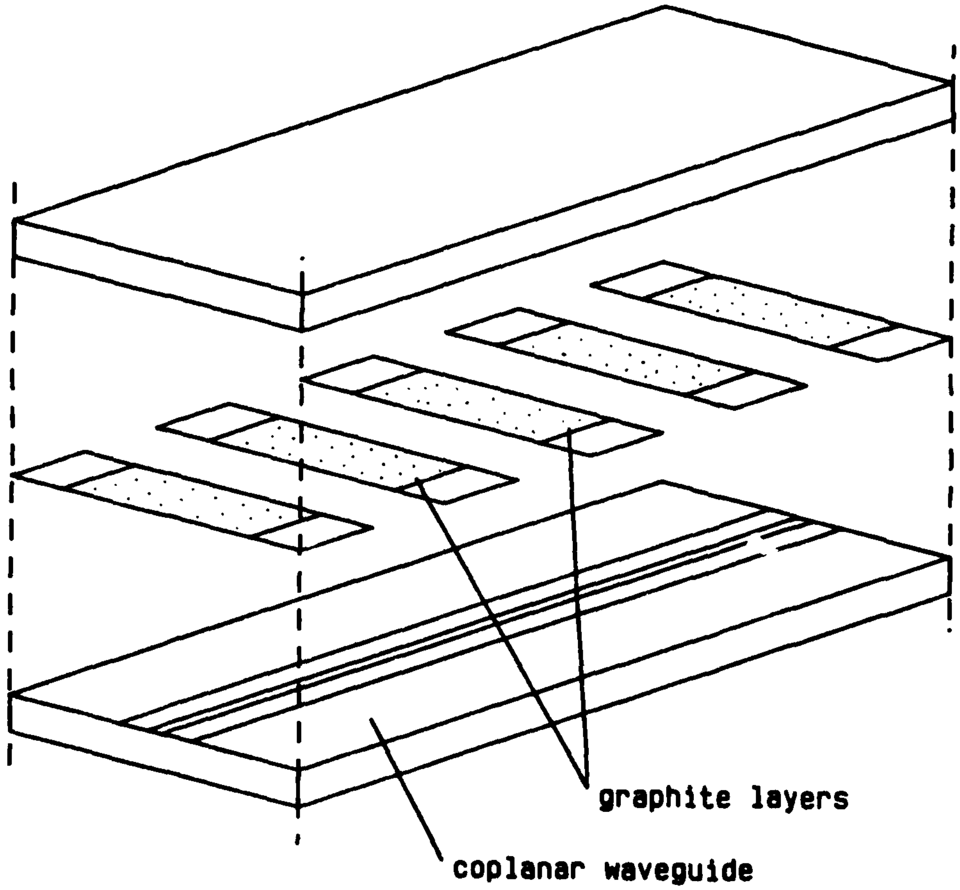

Figure 10 Schematic view of the experimental model of the MIS periodic coplanar waveguide

Table 2 Dimensions and material constants of the experimental models

common parameters		
total length of line		212 mm
width of center conductor	(2a)	2.0 mm
width of slot	(b-a)	4.0 mm
thickness of substrate	(d_3)	3.0 mm
dielectric constants	(ε_1, ε_2 and ε_4)	2.5 ε_o
MIS periodic coplanar waveguide		
thickness of insulator	(d_1)	0.13 mm
thickness of graphite layer	(d_2)	0.02 mm
length of each section	(ℓ_1 and ℓ_2)	8.0 mm
number of periods		12
Uniform MIS coplanar waveguide		
thickness of insulator	(d_1)	0.18 mm
thickness of graphite layer	(d_2)	0.02 mm

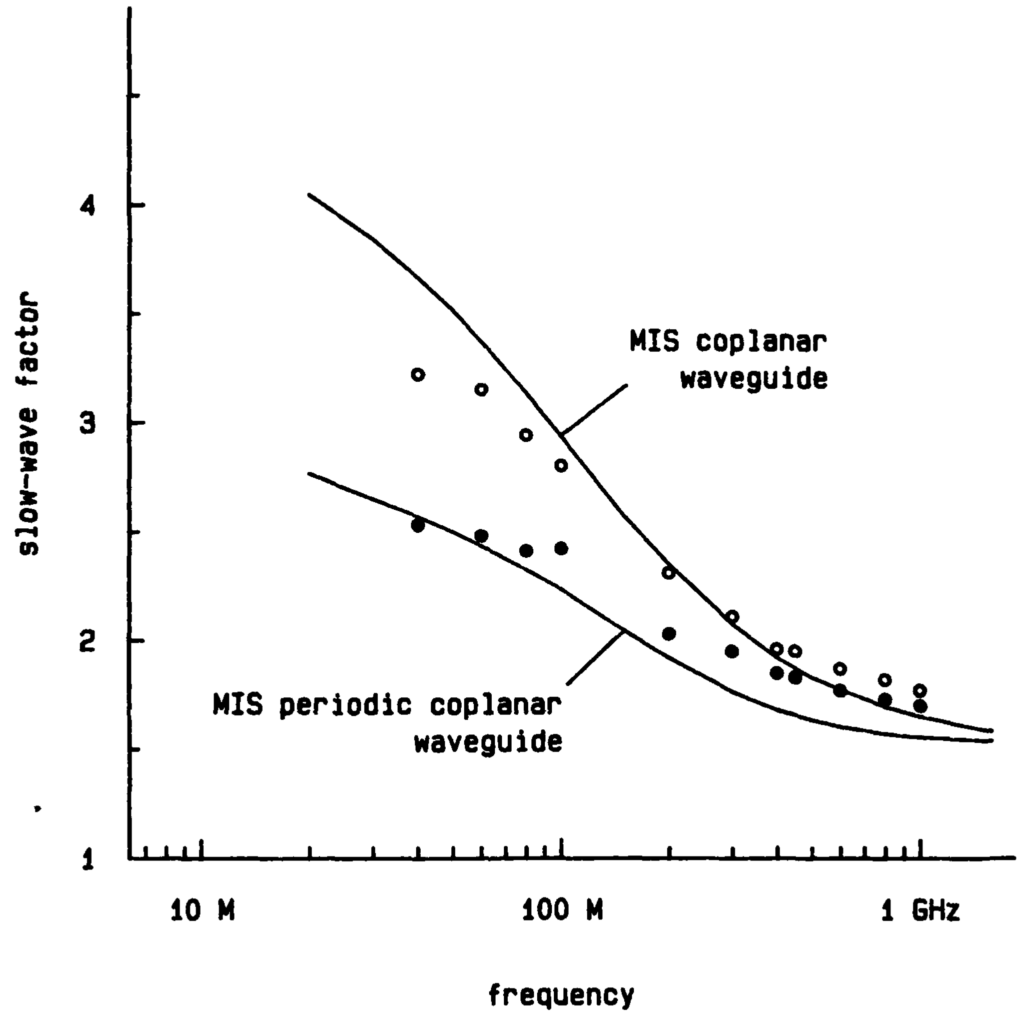

Figure 11a Comparison between experiment and theory : slow-wave factor

o ● : experimental results

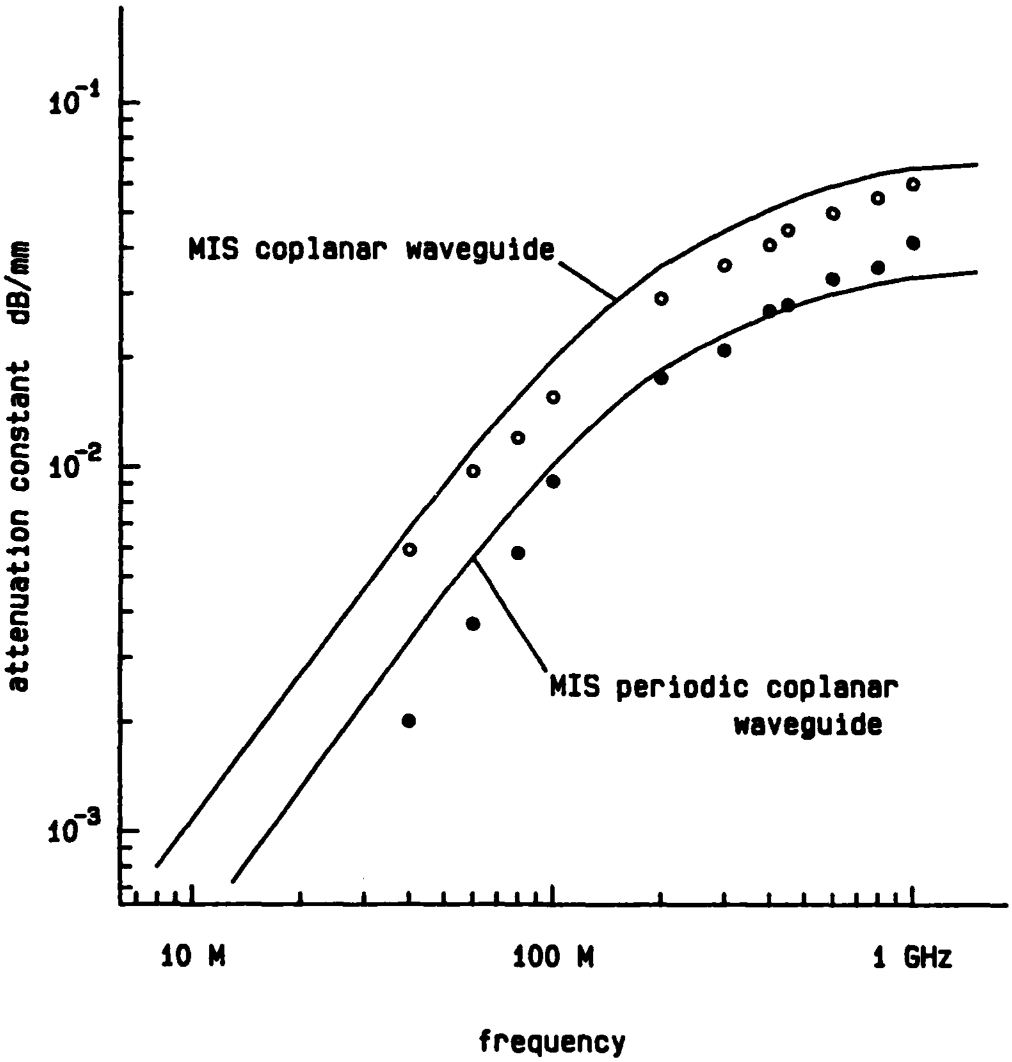

Figure 11b Comparison between experiment and theory : attenuation constant

o • : experimental results

agreement with the theoretical curves. The crossover of the slow-wave factor does not occur in this case since the conductivity of the graphite powder is too small. However, this experiment verifies the theoretical calculations, and the extension of the slow-wave propagation range is expected if appropriate conductivity is obtained.

CHAPTER 5 : COPLANAR SCHOTTKY VARIABLE PHASE SHIFTER

In this chapter, discuss a Schottky-contact coplanar waveguide as a variable phase shifter is discussed. This device can be constructed so that the center conductor of the coplanar waveguide forms a Schottky contact with a highly doped semiconductor substrate. Applying a proper dc bias voltage forms a depletion layer at the contact, which has a much smaller conductivity than the surrounding region. This situation is similar to the MIS coplanar waveguide, and slow-wave propagation is expected on such a line (Fig. 12). Since the depletion layer thickness can be controlled by changing the dc bias voltage on the center conductor of the coplanar waveguide, there is the possibility of making a electronically variable phase shifter using this configuration.

The theoretical discussion so far shows that the MIS coplanar waveguide has a higher attenuation coefficient at high frequencies. The slow-wave nature also disappears as the operating frequency becomes higher. However, the periodic structure proposed in the previous chapter has the advantage of reducing the attnuation constant and extending the slow-wave frequency region. The idea of making periodically doped sections on the semiconductor substrate can also be used in the Schottky-contact coplanar waveguide, which may reduce the attenuation and enhance the performance of the variable phase shifter.

In the present chapter, the previously developed numerical method will be used to determine the optimum operating conditions for both

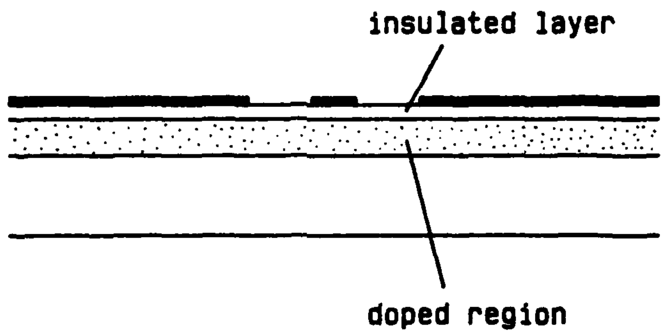

(a)

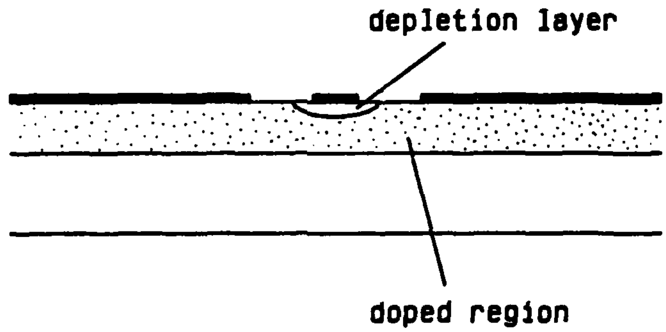

(b)

Figure 12 a MIS coplanar waveguide

b Schottky coplanar waveguide

uniform and periodic Schottky-contact coplanar waveguides as electronically variable phase shifters. The theory, however, can not be directly applied to these structures since they have curved boundaries at the bottom of the depletion layers. In order to be able to utilize the theoretical method, it is necessary to model the Schottky-contact coplanar waveguide by the MIS coplanar waveguide with the insulated layer having the same hight as the depletion layer of the Schottky contact. Since the depletion layer is very thin and the field is mostly confined under the center conductor, the error introduced by this model is considered to be small. Therefore, the performance of the electronically variable phase shifter can be studied by this method.

CONDITIONS OF OPTIMUM OPERATION

The important parameters to be considered for an optimum operating condition are the dimensions of the coplanar waveguide, the conductivity and the thickness of the doped region, and the depletion layer thickness. The relation between the dc bias voltage V and the thickness of the depletion layer d_1 can be calculated by the well known result [5]:

$$d_1 = \left[\frac{2\varepsilon}{qN_d} (V + V_D) \right]^{1/2} \qquad (19)$$

where ε is a permittivity, q the unit charge, N_d the doping concentration of impurities, V applied bias voltage, and V_D diffusion potential of the

Schottky barier. For GaAs substrate, this relation is plotted in Fig. 13. It is known that, at a fixed frequency, there is a certain value of the conductivity of the doped region that yields a maximum range of slow-wave frequency region [12]. This was also calculated in chapter 2. This value of the conductivity also gives the minimum attenuation over the range of conductivities. Therefore, it is important to choose an impurity concentration of the doped region so that the conductivity of this region becomes this optimum value. However, the impurity level is limited to a certain value, because the breakdown voltage becomes low when the impurity concentration is large. In Fig. 13, the dotted line indicates the critical voltage to cause the breakdown in the depletion layer, which is obtained by using a known value of breakdown electric field intensity, $E_B \simeq 4\times10^7$ V/m [20]. For this reason, a useful value of the conductivity of the doped region in GaAs substrate is limited up to 10^4 or 10^5 S/m.

Fig. 14 shows the behavior of the optimum conductivity at 10 GHz. Three curves are drawn to show the effect of the thickness of the doped region d_2. It is interesting that increased value of d_2 shifts the point of minimum attenuation to the left, i.e., the optimum conductivity is lowered. Also the minimum value of the attenuation constant is slightly lowered. Therefore it is necessary to set d_2 to a proper value. This tendency, however, disappears when d_2 exceeds a certain value, e.g., 10 μm in this case. The attenuation constant also depends on the width of the center conductor and the slot. Fig. 15 shows this dependence. The relation is simple: the narrower the widths, the lower the attenuation. However the calculation does not include the effect of con-

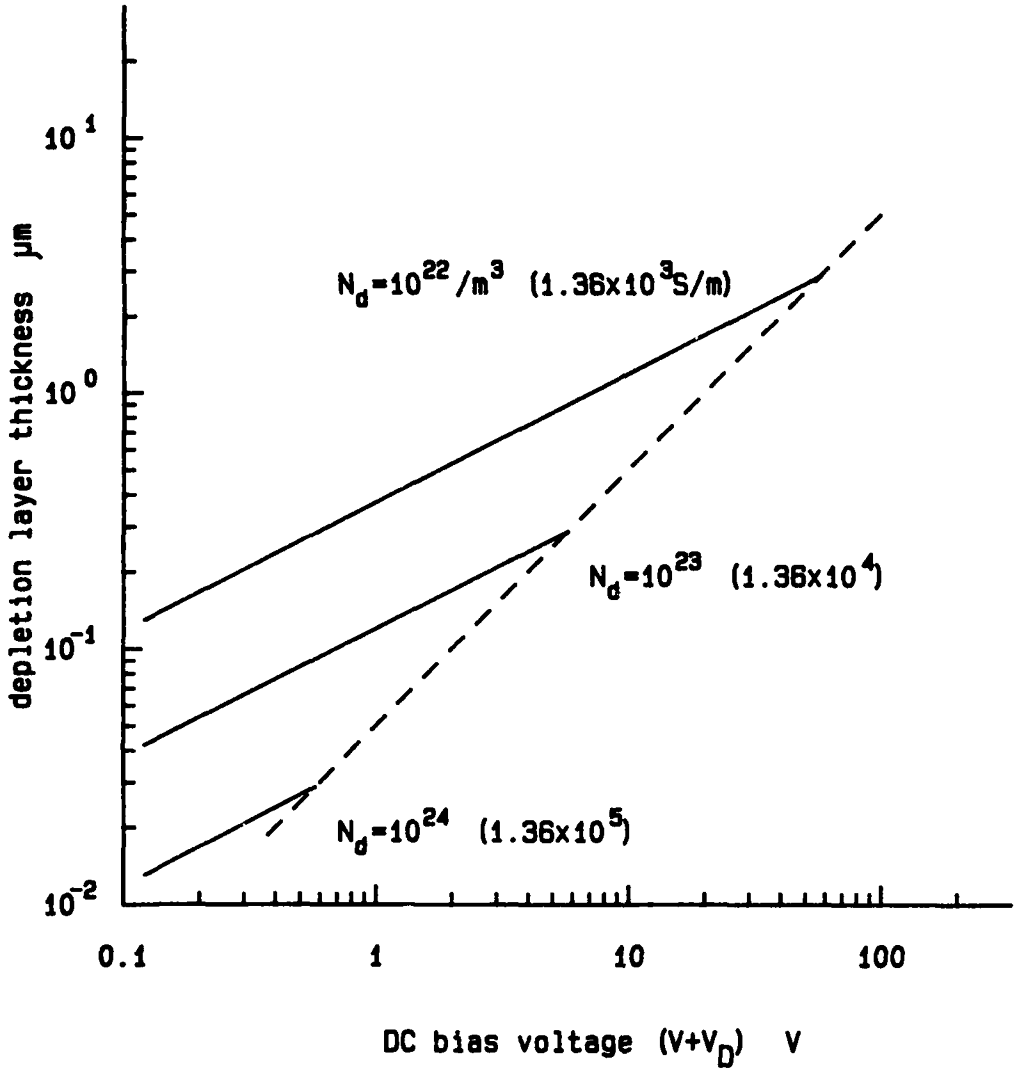

Figure 13 Depletion layer thickness versus DC bias current for GaAs substrate : Dotted line indicates the critical voltage.

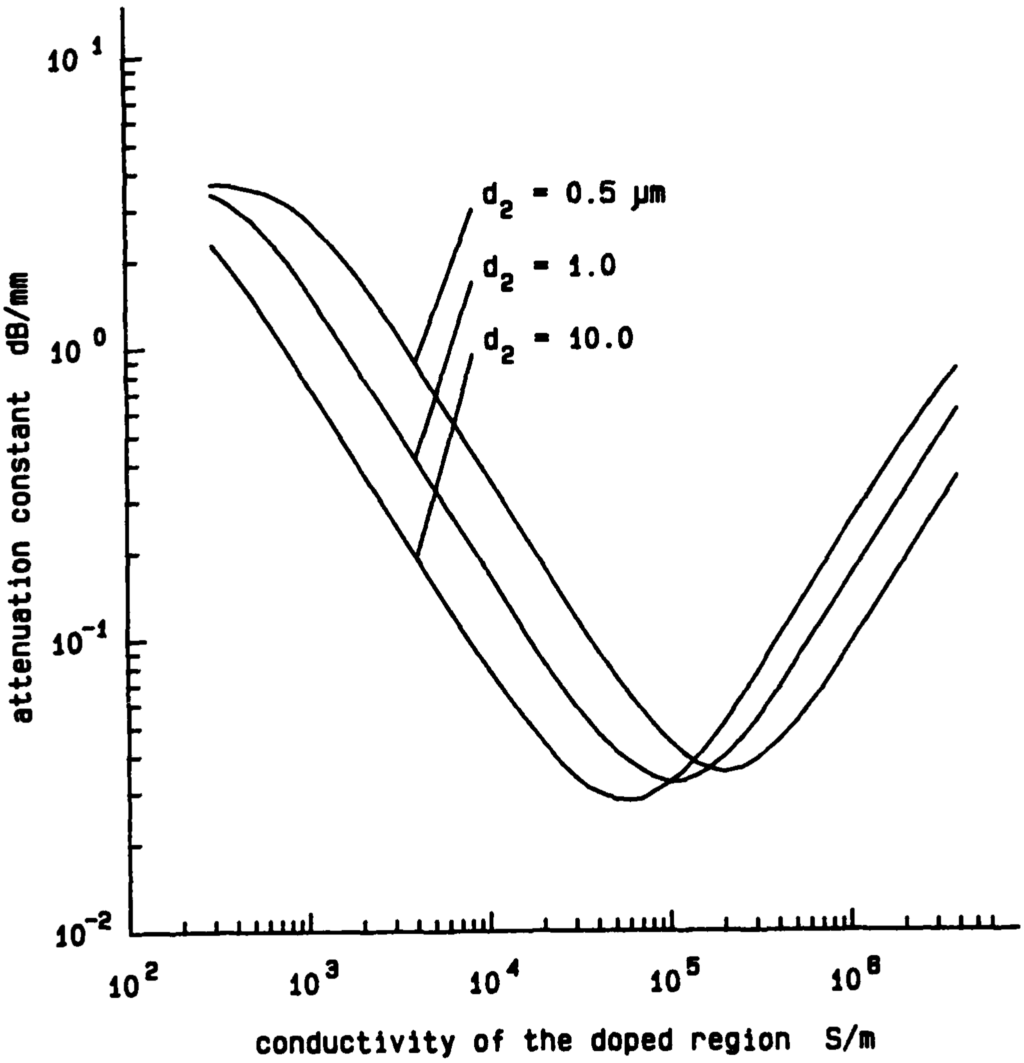

Figure 14 Behavior of the optimum conductivity

f = 10 GHz

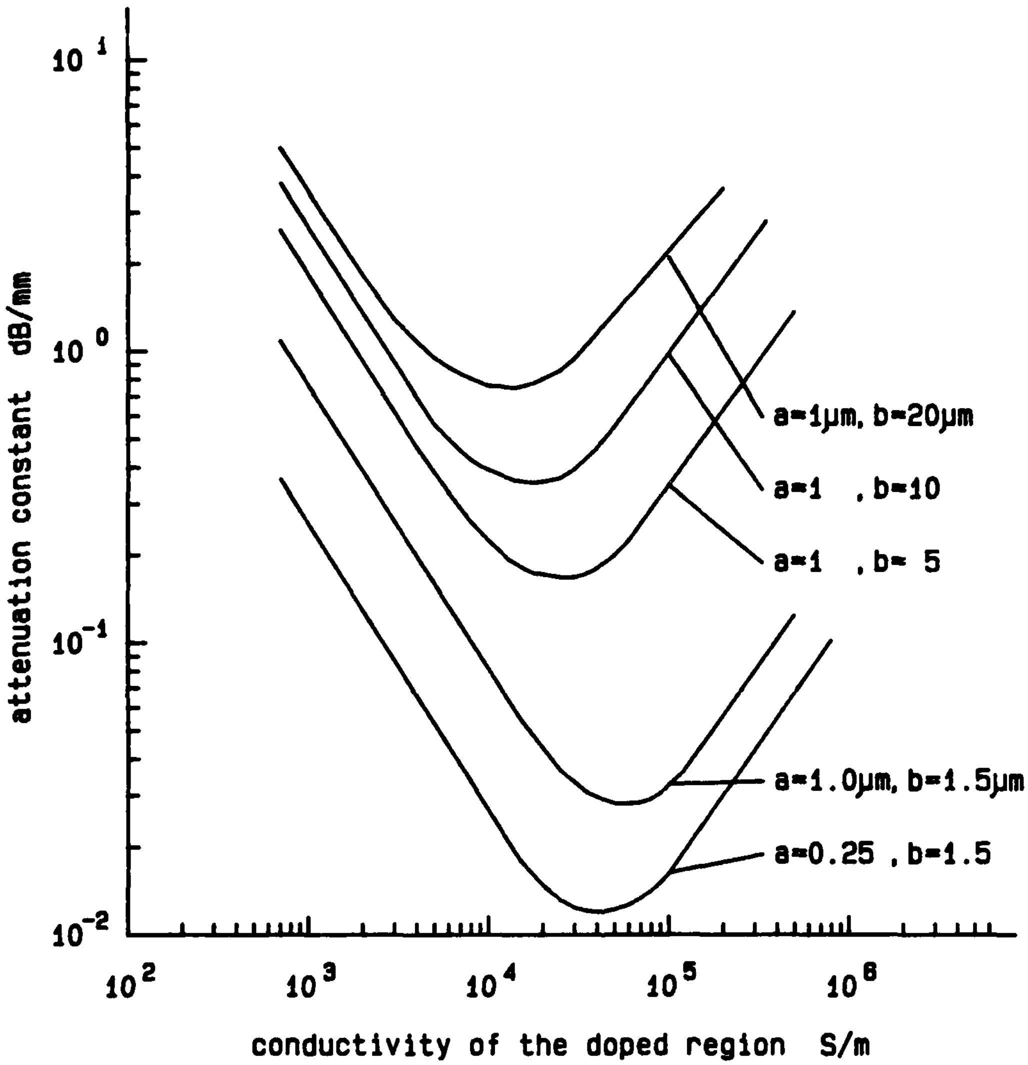

Figure 15 Behavior of the optimum conductivity

f = 10 GHz

ductor loss, and it is expected that having a very narrow center conductor causes large attenuation. Also, there is a lower limit on the slot width because the breakdown voltage of the semiconductor substrate becomes smaller for narrower slots.

There is one more parameter to consider: depletion layer thickness d_1. The thickness d_1 is determined by the dc bias voltage, and as was discussed earlier, it changes the phase shift of the device. However, it also changes the attenuation constant. This is inherent to this structure, but it is desirable to keep this change as small as possible. Fig. 16 is drawn for 2 different values of d_1. The figure shows that the small values of d_1 yields large attenuation. Also, the point of minimum attenuation moves as d_1 changes. This means that we would like to use point A in the figure rather than B to keep the total change in the attenuation small.

RESULTS

According to the above discussion, a model can be constructed for the optimum operation of a Schottky variable phase shifter. A GaAs substrate is chosen because of its large electron mobility and breakdown electric field intensity. Various constants for GaAs substrate used in the calculation are shown in Table 3. The width of the center conductor of the coplanar waveguide is chosen to be 2 μm (a=1 μm). In this case, the doping density in the doped region is $N_d=3\times10^{23}$ /m³, which yields a conductivity of $\sigma_3=4.1\times10^4$ S/m. This gives the lowest attenuation and a

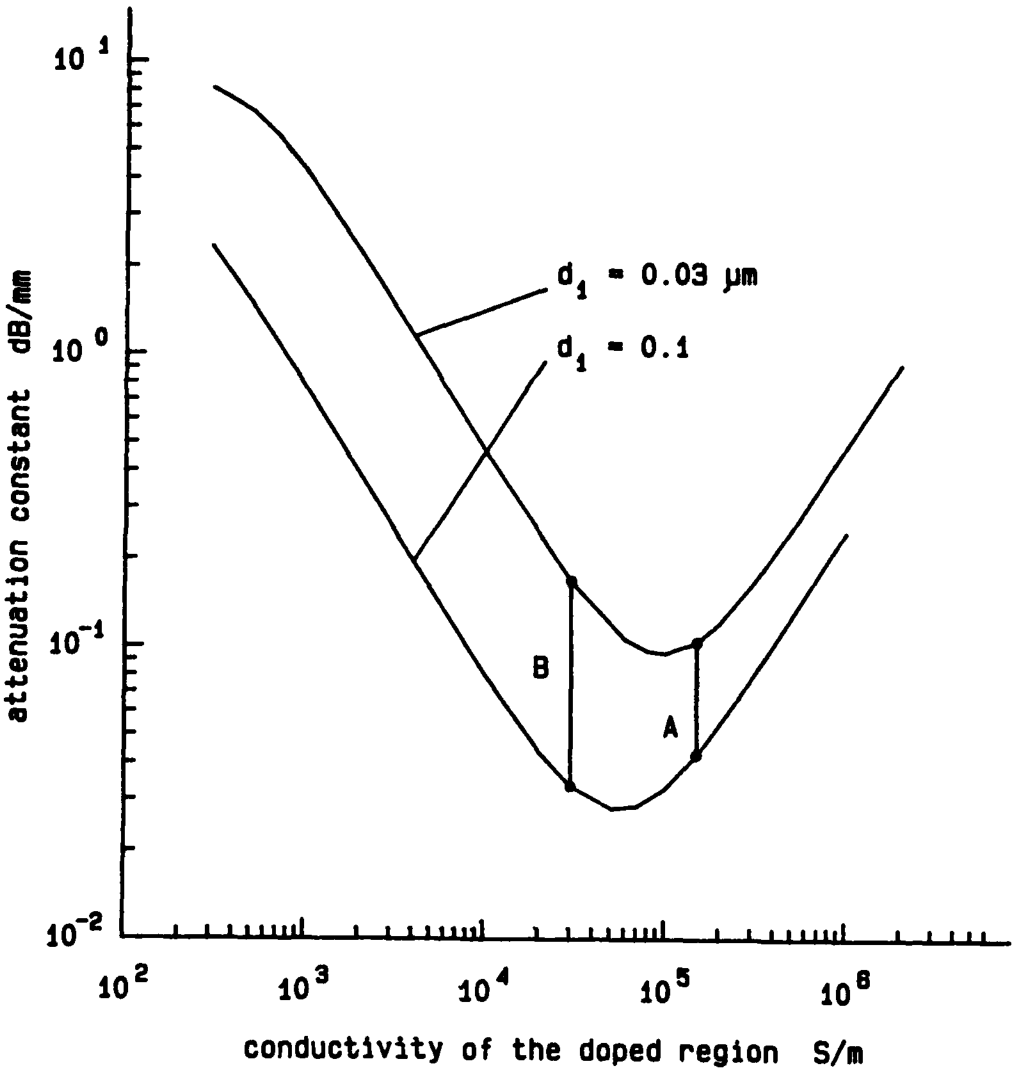

Figure 16 Attenuation constant versus conductivity of the doped region : Point A is better than B since the attenuation varies less. f = 10 GHz

Table 3 Various constants for GaAs substrate used in the calculation

dielectric constant	13.0
mobility	8500 $cm^2/V\text{-}sec$
breakdown field intensity	4.0×10^7 V/m
impurity density (doped region)	3.0×10^{23} $/m^3$
depth of doped region (d_2)	10 μm

calculated maximum depletion layer thickness of d_{1max}=0.12 μm when the dc bias voltage is $V+V_D$=1.9 V. This is the maximum voltage that can be applied in this situation (breakdown voltage).

Using these values, the required length of the device and the total attenuation in the device are calculated. The depth of the depletion layer is varied from 0.03 to 0.09 μm, which corresponds to adjusting $V+V_D$ from 0.2 to 1.7 V. The device length is determined so that the difference in phase of the output signal becomes 180 degrees when the dc bias voltage is changed from minimum to maximum value (0.2 to 1.7 V). The results are shown in Fig. 17. This figure is drawn as follows; for each value of b, the total device length required for 180 degree phase shift is calculated based on the propagation constant obtained by our theoretical calculation. The total attenuation in the device is then obtained by multiplying the maximum attenuation constant for the operating condition by the device length. The curves show that when the slot width becomes narrower, the total attenuation becomes smaller in spite of the longer device length required. The figure also shows that the total attenuation is smaller for the periodic structure compared to the uniform device. However, this advantage becomes less when the slot width becomes very narrow. The performance of the periodic structure could have been much better if the conductivity of the doped region were higher. We could not do this because of the low breakdown voltage of GaAs. Also, because of the same limitation, we can not meet the last condition given in the previous section: minimize the variation of the attenuation constant over the operating dc bias voltage. Therefore, if a better substrate material were used (i.e. one with high elec-

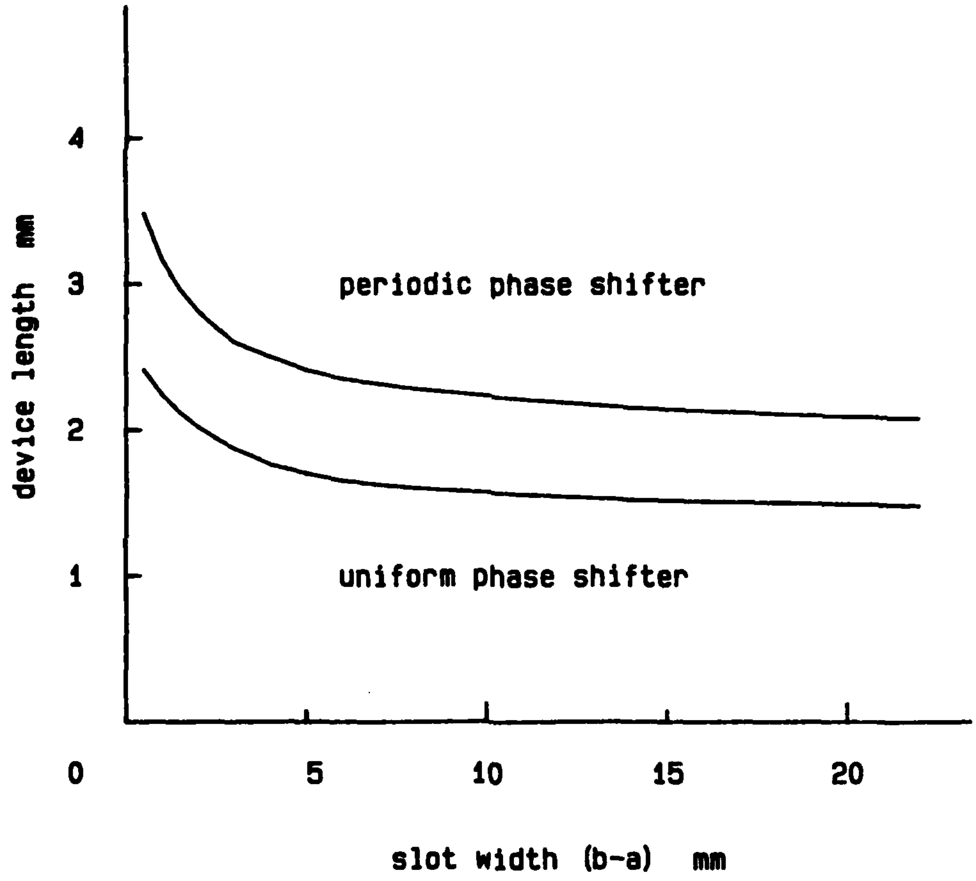

Figure 17a Required device length for various slot width $a = 1.0\ \mu m$, Parameters for GaAs substrate are shown in Table 1-3.

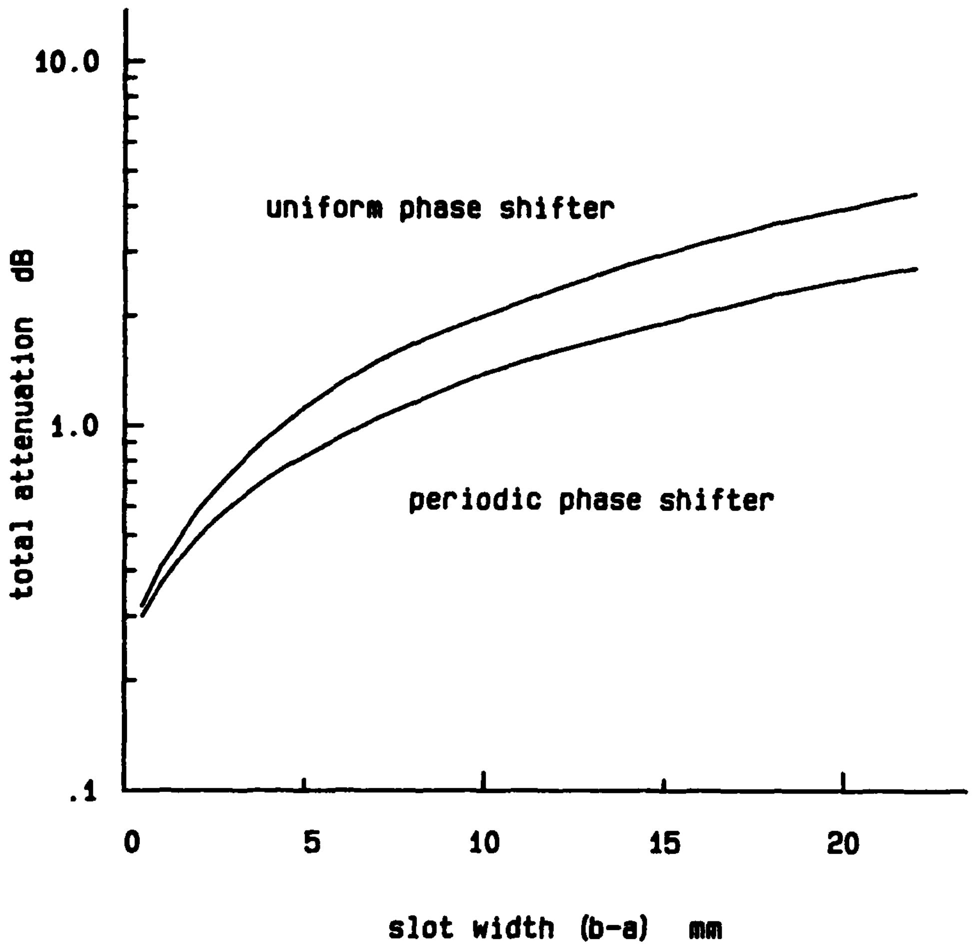

Figure 17b Total attenuation of the device
$a = 1.0\ \mu m$, Parameters for GaAs substrate are shown in Table 1-3.

tron mobility and breakdown electric field), an improvement of the performance of the periodic variable phase shifter would be possible.

Finally, the total attenuation of the device is plotted as a function of the frequency in Fig. 18. For a fixed frequency, the required device length is calculated and the total attenuation is then computed for that length. At 40 GHz, the calculated total attenuation is 1.27 dB for uniform device and 1.20 dB for the periodic device. Although these figures do not include conductor loss, they indicate quite satisfactory performance of these devices at millimeter-wave frequencies.

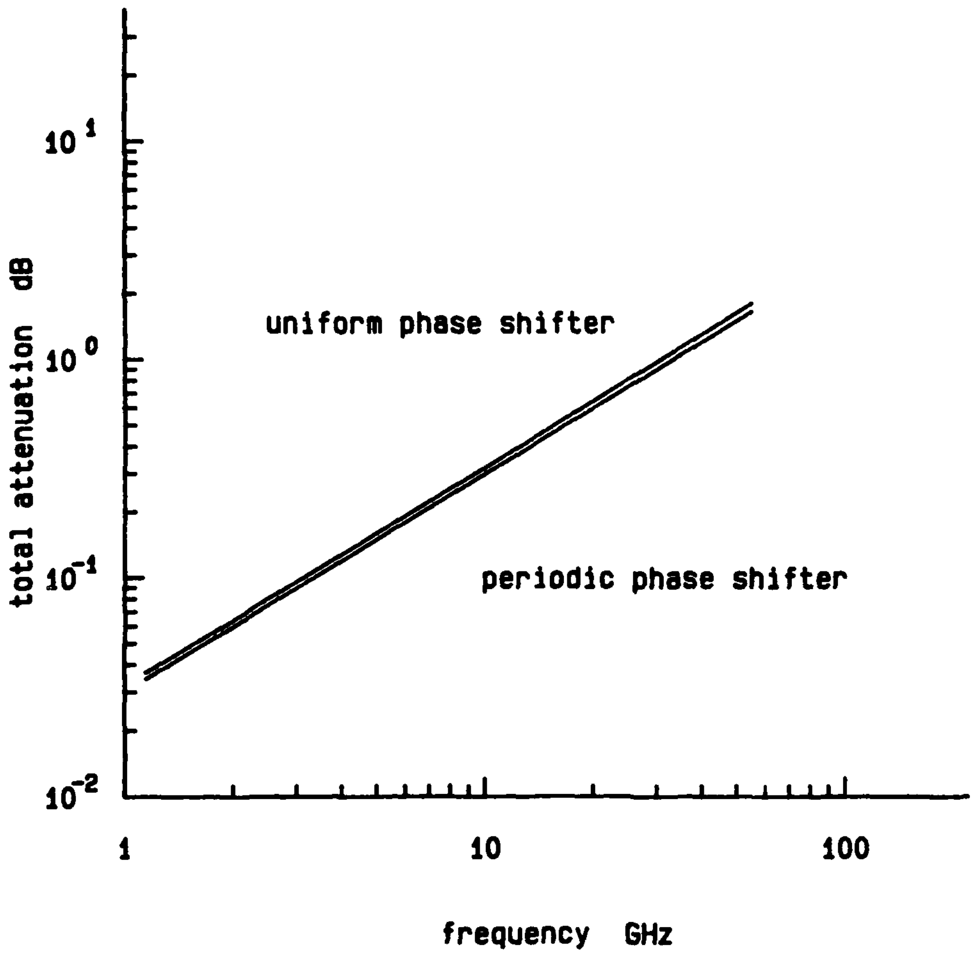

Figure 18 Total attenuation versus frequency

a = 1.0 μm, b = 1.5 μm

Parameters for GaAs substrate are shown

in Table 1-3.

CHAPTER 6 : CONCLUSIONS

In Part I, the theoretical development of the coplanar, Schottky variable phase shifter has been accomplished. An efficient computer program was developed to calculate the trasmission-line parameters of the MIS slow-wave coplanar waveguide. In order to reduce the inherent loss in such a device, a periodic structure was proposed and analyzed by conventional transmission-line theory. A simple experiment verified the applicability of this method. Extensive calculations were performed to find the optimum conditions of the phase shifters based on the GaAs substrate. Calculations show that optimized 180-degree phase shifter can be operated at 40 GHz with a loss as small as 1.2 dB.

APPENDIX A : DERIVATION OF THE INTEGRAL EQUATION

In Appendix A, a detailed derivation of the integral equation (14) will be given. The potentials ψ and ϕ in each region are given by eq. (7) through (11). Using these expressions, we can satisfy all the boundary conditions to obtain the integral equation (14). To do so, we need to utilize eqs. (5) and (6), which can be rewritten as

$$E_x = \frac{1}{j\omega\varepsilon} \frac{\partial^2 \psi}{\partial x \partial y} - j\gamma\phi$$

$$E_y = \frac{1}{j\omega\varepsilon} \left(k^2 + \frac{\partial^2}{\partial y^2} \right) \psi$$

$$E_z = - \frac{\gamma}{\omega\varepsilon} \frac{\partial\psi}{\partial y} - \frac{\partial\phi}{\partial x}$$

$$H_x = j\gamma\psi + \frac{1}{j\omega\mu} \frac{\partial^2 \phi}{\partial x \partial y}$$

$$H_y = \frac{1}{j\omega\mu} \left(k^2 + \frac{\partial^2}{\partial y^2} \right) \phi$$

$$H_z = \frac{\partial\psi}{\partial x} - \frac{\gamma}{\omega\mu} \frac{\partial\phi}{\partial y}$$

(A-1)

The boundary conditions to be satisfied is the continuity of the x and z components of the electric and magnetic fields (E_x, E_z, H_x, and H_z) at $y=-d_1$, $-d_1-d_2$, and $-d_1-d_2-d_3$. For example, at $y=-d_1$,

$$E_x = -\frac{1}{j\omega\varepsilon_2} \sum_n \alpha_{2n} \beta_n \sin\beta_n x \left(C_n \cos\alpha_{2n} d_1 + C_n' \sin\alpha_{2n} d_1 \right)$$

$$- j\gamma \sum_n \sin\beta_n x \left(- D_n \sin\alpha_{2n} d_1 + D_n' \cos\alpha_{2n} d_1 \right)$$

$$= \frac{1}{j\omega\varepsilon_3} \sum_n - \alpha_{3n} \beta_n \sin\beta_n x\, E_n - j\gamma \sum_n \sin\beta_n x\, F_n'$$

$$E_z = -\frac{\gamma}{\omega\varepsilon_2} \sum_n \alpha_{2n} \cos\beta_n x \,(C_n \cos\alpha_{2n}d_1 + C_n' \sin\alpha_{2n}d_1)$$

$$- \sum_n \beta_n \cos\beta_n x \,(- D_n \sin\alpha_{2n}d_1 + D_n' \cos\alpha_{2n}d_1)$$

$$= -\frac{\gamma}{\omega\varepsilon_3} \sum_n \alpha_{3n} \cos\beta_n x \, E_n - \sum_n \beta_n \cos\beta \, F_n'$$

$$H_x = j\gamma \sum_n \cos\beta_n x \,(- C_n \sin\alpha_{2n}d_1 + C_n' \cos\alpha_{2n}d_1)$$

$$+ \frac{1}{j\omega\mu} \sum_n \alpha_{2n} \beta_n \cos\beta_n x \,(D_n \cos\alpha_{2n}d_1 + D_n' \sin\alpha_{2n}d_1)$$

$$= j\gamma \sum_n \cos\beta_n x \, E_n' + \frac{1}{j\omega\mu} \sum_n \alpha_{3n} \beta_n \cos\beta_n x \, F_n$$

$$H_z = - \sum_n \beta_n \sin\beta_n x \,(- C_n \sin\alpha_{2n}d_1 + C_n' \cos\alpha_{2n}d_1)$$

$$- \frac{\gamma}{\omega\mu} \sum_n \alpha_{2n} \sin\beta_n x \,(D_n \cos\alpha_{2n}d_1 + D_n' \sin\alpha_{2n}d_1)$$

$$= - \sum_n \beta_n \sin\beta_n x \, E_n' - \frac{\gamma}{\omega\mu} \sum_n \alpha_{3n} \sin\beta_n x \, F_n \qquad \text{(A-2)}$$

From these relations, we obtain

$$\begin{bmatrix} \Gamma_{11}^{(1)} & \Gamma_{12}^{(1)} \\ \Gamma_{21}^{(1)} & \Gamma_{22}^{(1)} \end{bmatrix} \begin{bmatrix} C_n \\ C_n' \end{bmatrix} = \begin{bmatrix} E_n \\ E_n' \end{bmatrix} \tag{A-3}$$

$$\begin{bmatrix} \Gamma_{11}^{(2)} & \Gamma_{12}^{(2)} \\ \Gamma_{21}^{(2)} & \Gamma_{22}^{(2)} \end{bmatrix} \begin{bmatrix} D_n \\ D_n' \end{bmatrix} = \begin{bmatrix} F_n \\ F_n' \end{bmatrix} \tag{A-4}$$

where

$$\Gamma_{11}^{(1)} = \frac{\varepsilon_3}{\varepsilon_2} \frac{\alpha_{2n}}{\alpha_{3n}} \cos\alpha_{2n} d_1$$

$$\Gamma_{12}^{(1)} = \frac{\varepsilon_3}{\varepsilon_2} \frac{\alpha_{2n}}{\alpha_{3n}} \sin\alpha_{2n} d_1$$

$$\Gamma_{21}^{(1)} = - \sin\alpha_{2n} d_1$$

$$\Gamma_{22}^{(1)} = \cos\alpha_{2n} d_1$$

$$\Gamma_{11}^{(2)} = \frac{\alpha_{2n}}{\alpha_{3n}} \cos\alpha_{2n} d_1$$

$$\Gamma_{12}^{(2)} = \frac{\alpha_{2n}}{\alpha_{3n}} \sin\alpha_{2n}d_1$$

$$\Gamma_{21}^{(2)} = - \sin\alpha_{2n}d_1$$

$$\Gamma_{22}^{(2)} = \cos\alpha_{2n}d_1$$

Similarly, from the boundary conditions at $y=-d_1-d_2$ and $-d_1-d_2-d_3$, we obtain

$$\begin{bmatrix} \Gamma_{11}^{(3)} & \Gamma_{12}^{(3)} \\ \Gamma_{21}^{(3)} & \Gamma_{22}^{(3)} \end{bmatrix} \begin{bmatrix} E_n \\ E_n' \end{bmatrix} = \begin{bmatrix} G_n \\ G_n' \end{bmatrix} \tag{A-5}$$

$$\begin{bmatrix} \Gamma_{11}^{(4)} & \Gamma_{12}^{(4)} \\ \Gamma_{21}^{(4)} & \Gamma_{22}^{(4)} \end{bmatrix} \begin{bmatrix} F_n \\ F_n' \end{bmatrix} = \begin{bmatrix} H_n \\ H_n' \end{bmatrix} \tag{A-6}$$

$$\begin{bmatrix} \Gamma_{11}^{(5)} & \Gamma_{12}^{(5)} \end{bmatrix} \begin{bmatrix} G_n \\ G_n' \end{bmatrix} = 0 \tag{A-7}$$

$$\begin{bmatrix} \Gamma_{11}^{(6)} & \Gamma_{12}^{(6)} \end{bmatrix} \begin{bmatrix} H_n \\ H_n' \end{bmatrix} = 0 \tag{A-8}$$

where

$$\Gamma_{11}^{(3)} = \frac{\varepsilon_4}{\varepsilon_3} \frac{\alpha_{3n}}{\alpha_{4n}} \cos\alpha_{3n} d_2$$

$$\Gamma_{12}^{(3)} = \frac{\varepsilon_4}{\varepsilon_3} \frac{\alpha_{3n}}{\alpha_{4n}} \sin\alpha_{3n} d_2$$

$$\Gamma_{21}^{(3)} = - \sin\alpha_{3n} d_2$$

$$\Gamma_{22}^{(3)} = \cos\alpha_{3n} d_2$$

$$\Gamma_{11}^{(4)} = \frac{\alpha_{3n}}{\alpha_{4n}} \cos\alpha_{3n} d_2$$

$$\Gamma_{12}^{(4)} = \frac{\alpha_{3n}}{\alpha_{4n}} \sin\alpha_{3n} d_2$$

$$\Gamma_{21}^{(4)} = -\sin\alpha_{3n}d_2$$

$$\Gamma_{22}^{(4)} = \cos\alpha_{3n}d_2$$

$$\Gamma_{11}^{(5)} = \frac{1}{\varepsilon_4}\alpha_{4n}\cos\alpha_{4n}d_3 + \frac{1}{\varepsilon_5}\alpha_{5n}\sin\alpha_{4n}d_3$$

$$\Gamma_{12}^{(5)} = \frac{1}{\varepsilon_4}\alpha_{4n}\sin\alpha_{4n}d_3 - \frac{1}{\varepsilon_5}\alpha_{5n}\cos\alpha_{4n}d_3$$

$$\Gamma_{11}^{(6)} = \alpha_{4n}\cos\alpha_{4n}d_3 + \alpha_{5n}\sin\alpha_{4n}d_3$$

$$\Gamma_{12}^{(6)} = \alpha_{4n}\sin\alpha_{4n}d_3 - \alpha_{5n}\cos\alpha_{4n}d_3$$

Using (A-3), (A-5), and (A-7), we obtain

$$[\ \Gamma_{11}^{(5)}\ \Gamma_{12}^{(5)}\ ] \begin{bmatrix} \Gamma_{11}^{(3)} & \Gamma_{12}^{(3)} \\ \Gamma_{21}^{(3)} & \Gamma_{22}^{(3)} \end{bmatrix} \begin{bmatrix} \Gamma_{11}^{(1)} & \Gamma_{12}^{(1)} \\ \Gamma_{21}^{(1)} & \Gamma_{22}^{(1)} \end{bmatrix} \begin{bmatrix} C_n \\ C_n' \end{bmatrix} = 0$$

$$[\ \Gamma_{11}^{(6)}\ \Gamma_{12}^{(6)}\ ] \begin{bmatrix} \Gamma_{11}^{(4)} & \Gamma_{12}^{(4)} \\ \Gamma_{21}^{(4)} & \Gamma_{22}^{(4)} \end{bmatrix} \begin{bmatrix} \Gamma_{11}^{(2)} & \Gamma_{12}^{(2)} \\ \Gamma_{21}^{(2)} & \Gamma_{22}^{(2)} \end{bmatrix} \begin{bmatrix} D_n \\ D_n' \end{bmatrix} = 0$$

Therefore, we can obtain the ratio of C_n and C_n' as follows:

$$P_{cn} = \frac{C_n'}{C_n}$$

$$= - \frac{\Gamma_{11}^{(5)}(\Gamma_{11}^{(1)}\Gamma_{11}^{(3)}+\Gamma_{21}^{(1)}\Gamma_{12}^{(3)}) + \Gamma_{12}^{(5)}(\Gamma_{11}^{(1)}\Gamma_{21}^{(3)}+\Gamma_{21}^{(1)}\Gamma_{22}^{(3)})}{\Gamma_{11}^{(5)}(\Gamma_{12}^{(1)}\Gamma_{11}^{(3)}+\Gamma_{22}^{(1)}\Gamma_{21}^{(3)}) + \Gamma_{12}^{(5)}(\Gamma_{12}^{(1)}\Gamma_{21}^{(3)}+\Gamma_{22}^{(1)}\Gamma_{22}^{(3)})}$$

$$P_{dn} = \frac{D_n}{D_n'}$$

$$= - \frac{\Gamma_{11}^{(5)}(\Gamma_{12}^{(1)}\Gamma_{11}^{(3)}+\Gamma_{22}^{(1)}\Gamma_{21}^{(3)}) + \Gamma_{12}^{(5)}(\Gamma_{12}^{(1)}\Gamma_{21}^{(3)}+\Gamma_{22}^{(1)}\Gamma_{22}^{(3)})}{\Gamma_{11}^{(5)}(\Gamma_{11}^{(1)}\Gamma_{11}^{(3)}+\Gamma_{21}^{(1)}\Gamma_{12}^{(3)}) + \Gamma_{12}^{(5)}(\Gamma_{11}^{(1)}\Gamma_{21}^{(3)}+\Gamma_{21}^{(1)}\Gamma_{22}^{(3)})}$$

These are the coefficients appearing in eq. (12).

Next, by applying the boundary conditions on E_x and E_z at y=0, the following relations can be easily obtained.

$$C_n = - \frac{\varepsilon_2}{\varepsilon_1} \frac{\alpha_{1n}}{\alpha_{2n}} A_n$$

$$D_n' = B_n$$

Therefore the potentials in Region 2 can be written as in eq. (12).

In order to obtain the integral equation (14), we use the remaining boundary conditions in (13) and (15). Using the condition on E_{x1}, we obtain

$$E_{x1} = \frac{1}{j\omega\varepsilon_1} \sum_n A_n \alpha_{1n} \beta_n \sin\beta_n x - j\gamma \sum_n B_n \sin\beta_n x$$

$$\begin{aligned} &= 0 \qquad 0<x<a,\ b<x<w \\ &\quad f(x) \qquad a<x<b \end{aligned}$$

which, by the Fourier analysis, becomes

$$\frac{1}{j\omega\varepsilon_1} A_n \alpha_{1n} \beta_n - j\gamma B_n = \frac{2}{w} \int_a^b f(x) \sin\beta_n x \, dx \tag{A-9}$$

Similarly, using the condition on H_x,

$$j\gamma \left(1 + P_{cn} \frac{\varepsilon_2}{\varepsilon_1} \frac{\alpha_{1n}}{\alpha_{2n}} \right) A_n - \frac{1}{j\omega\mu} \left(P_{dn} \frac{\alpha_{2n}}{\alpha_{1n}} + 1 \right) B_n \alpha_{1n} \beta_n$$

$$= \frac{2}{w} \left(\int_0^a + \int_b^w \right) g(x) \cos\beta_n x \, dx \tag{A-10}$$

Using these results, we can obtain the coefficients An and Bn:

$$A_n = \frac{1}{V_n}\frac{2}{w}\left(\frac{1}{j\omega\mu} T_n \alpha_{1n} \beta_n \xi_n - j\gamma \zeta_n \right)$$

$$B_n = \frac{1}{V_n}\frac{2}{w}\left(j\gamma S_n \xi_n - \frac{1}{j\omega\varepsilon_1} \alpha_{1n} \beta_n \zeta_n \right)$$

where

$$V_n = \gamma^2 S_n - \frac{1}{\omega^2 \varepsilon_1 \mu} T_n \alpha_{1n}^2 \beta_n^2$$

$$S_n = 1 + P_{cn} \frac{\varepsilon_2}{\varepsilon_1} \frac{\alpha_{1n}}{\alpha_{2n}}$$

$$T_n = P_{dn} \frac{\alpha_{2n}}{\alpha_{1n}} + 1$$

$$\xi_n = \int_a^b f(x) \sin\beta_n x \, dx$$

$$\zeta_n = \left(\int_0^a + \int_b^w \right) g(x) \cos\beta_n x \, dx$$

We now substitute An and Bn into the rest of the boundary conditions:

$$E_{z1} = \sum_n \frac{1}{V_n} \{ (\frac{1}{\omega^2 \varepsilon_1 \mu} \alpha_{1n}^2 T_n + S_n) \beta_n \gamma \xi_n$$

$$+ (\gamma^2 + \beta_n^2) \frac{\alpha_{1n}}{\omega \varepsilon_1} \zeta_n \} \cos\beta_n x = 0$$

$0<x<a, \ b<x<w$

$$H_{z1} - H_{z2}$$

$$= - \sum_n A_n S_n \beta_n \sin\beta_n x + \frac{\gamma}{\omega\mu} \sum_n B_n T_n \alpha_{1n} \sin\beta_n x = 0$$

$a<x<b$

These relations can be rewritten as the integral equation (14) using the Fourier analysis:

$$\sum_n [P_n \int_s f(x') \sin\beta_n x' \, dx' + Q_n \int_c g(x') \cos\beta_n x' \, dx'] \cos\beta_n x = 0$$

$0<x<a, \ b<x<w$

$$\sum_n [R_n \int_s f(x') \sin\beta_n x' \, dx' + P_n \int_c g(x') \cos\beta_n x' \, dx'] \sin\beta_n x = 0$$

$a<x<b$

(1-14)

where

$$P_n = \frac{1}{V_n} \left(\frac{1}{\omega^2 \varepsilon_1 \mu} \alpha_{1n}^2 T_n + S_n \right) \beta_n \gamma$$

$$Q_n = \frac{1}{V_n} \left\{ \left(\gamma^2 + \beta_n^2 \right) \frac{\alpha_{1n}}{\omega \varepsilon_1} \right\}$$

$$R_n = \frac{1}{V_n} \left(\gamma^2 + \beta_n^2 \right) \frac{1}{\omega \mu} S_n T_n \alpha_{1n}$$

APPENDIX B : PROGRAM LISTING

Appendix B contains the FORTRAN program code for the analysis of the propagation characteristics of the uniform and periodic MIS coplanar waveguide. The subprograms CGECO, CGEDI, CGESL, and CSVDC are found in the LINPACK library, and ZANLYT is found in the IMSL library in The University of Texas Numerical Analysis Library.

```
      PROGRAM CPWINT(TTY,OUTPUT,TAPE1,TAPE5=TTY,TAPE6=TTY)
C
C
C
C        COMPUTATION OF THE COMPLEX PROPAGATION CONSTANT
C               OF THE UNIFORM AND PERIODIC MIS
C                      COPLANAR WAVEGUIDE
C
C
C
C        STRUCTURE :
C
C        THE RIGHT HALF OF THE CROSS SECTION OF THE
C        STRUCTURE IS SHOWN BELOW
C
C
C        : M. WALL (CENTER)                 : E. WALL
C        :                                  :
C        :           EPS1 (AIR)             :
C        :                                  :
C        :< - - - - - - -  W - - - - - - - >:
C        :< - - B - - >                     :
C        :< - A - >                         :
C        :=========-----====================:
C     D1 :       EPS2 (INSULATOR)           :
C        :----------------------------------:
C     D2 :     EPS3,SIG3 (DOPED REGION)     :
C        :----------------------------------:
C     D3 :       EPS4 (SEMI-INSULATED)      :
C        :----------------------------------:
C        :           EPS5 (AIR)             :
C        :                                  :
C
C
C
C        A  ...   HALF WIDTH OF CENTER STRIP
C        B  ...   A + WIDTH OF SLOT
C        W  ...   HALF WIDTH OF OUTER GUIDE
C        D1 ...   THICKNESS OF INSULATOR
C        D2 ...   THICKNESS OF DOPED REGION
C        D3 ...   THICKNESS OF SI SUBSTRATE
C
C        MMAX ...  NUMBER OF TERMS IN SUMMATIONS
C        NP   ...  NUMBER OF POINTS TO EVALUATE
C                  INTEGRAL
C
C        SOME VARIABLES ARE PRESET BY THE PROGRAM TO
C        CERTAIN VALUES (GAAS IS ASSUMED).   WHEN YOU
C        START CALCULATION FOR A DIFFERENT STRUCTURE,
C        CONVERGENCE OF THE SOLUTIONS SHOULD BE INVESTI-
C        GATED BY CHANGING THE VALUES OF MMAX AND NP.
C        ( MMAX .LE. 1200,  NP .LT. 50 )
C
C        THE SOLUTION IS OBTAINED BY EVALUATING THE
C        DETERMINANT OF THE MATRIX Z IN FUNCTION SUB-
C        PROGRAM DETERM.   THE ACCURACY OF THIS METHOD
C        CAN BE CHECKED BY CHOOSING THE OPTION 7 AFTER
C        THE CALCULATION OF THE PROPAGATION CONSTANT.
C        IT USES THE SINGULAR VALUE DECOMPOSITION
C        TO ACCURATELY EVALUATE THE CONDITION NUMBER OF
C        THE MATRIX.   3 CONDITION NUMBERS ARE CALCULATED
C        BY THE PROGRAM (RCOND).   THE 1ST ONE SHOULD BE
```

```
C         MUCH SMALLER THAN THE REST OF THEM.
C
C
C         LIBRARIES :
C            AALIB (CGECO, CGEDI, CGESL, CTAN, PHASE,
C                   CSVDC, CSROT)
C            IMSLIBF (ZANLYT)
C
C
      COMMON    /BLOCK0/A, B, W, D1, D2, D3, AKO, PI, ZMU, ZEP, OMEGA
      COMMON    /BLOCK1/EPS1, EPS2, ZEPS3, EPS4, EPS5
      COMMON    /BLOCK2/BETA(1200)
      COMMON    /BLOCK3/MMAX, NP, J1, J2, J3, IIMP, IFACT, ZIMP
      COMMON    /BLOCK4/X(50), XP(50)
      COMPLEX   ZEPS3, ZJ, DETERM
      COMPLEX   ZDET, ZC(2), ZIMP, CX(2), PCONST(2)
      REAL      L(2), TG(4)
      DIMENSION INFER(2)
      EXTERNAL  DETERM
C
C         BASIC CONSTANTS.
C
      ZJ = (0.0, 1.0)
      PI = 3.1415926535897
      ZMU = 4.0E-7 * PI
      ZEP = 8.854E-12
      DBN = 8.6859E-3
C
      IFLAG1 = 0
      IFLAG2 = 0
      IFLAG3 = 0
      ISECTN = 1
      EPS1 = 1.0
      EPS2 = 13.0
      EPS3 = 13.0
      EPS4 = 13.0
      EPS5 = 1.0
      MMAX = 500
      NP = 25
      G = 2.0
      DO 1 I=1,4
      TG(I) = 0.0
    1 CONTINUE
      ZC(1) = (0.0,0.0)
      ZC(2) = (0.0,0.0)
      SIG3 = 0.0
      FREQ = 0.0
      MMIN = 0
      GAM = 0.0
      ATTEN = 0.0
      SHIFT = 0.0
C
C         MAIN CONTROL.
C
 1000 WRITE (6,100)
  100 FORMAT ( 5/,5X,'****** MAIN MENU *****'
     1 //5X,'1  ...   CALCULATION OF MIS COPLANAR WAVEGUIDE'
     2 /5X,'2  ...  CALCULATION OF PERIODIC STRUCTURE'
     3 /5X,'10 ...  STOP' )
      READ (5, * )  ICTRL
      IF ( ICTRL .EQ. 1 )  GO TO 2000
      IF ( ICTRL .EQ. 2 )  GO TO 4000
```

```
      IF ( ICTRL .EQ. 10 )  STOP
      WRITE (6,110)
  110 FORMAT ( '?' )
      GO TO 1000
C
C          CALCULATION OF MIS COPLANAR WAVEGUIDE.
C
 2000 IF ( IFLAG1 .EQ. 0 )  GO TO 2100
      WRITE (6,120)  MMAX,NP,G,J1,J2,J3,MMIN,
     1               EPS1,EPS2,EPS3,EPS4,EPS5,
     2               A,B,W,D1,D2,D3,SIG3,FREQ
  120 FORMAT ( 5/,5X,'****** MIS COPLANAR WAVEGUIDE ******'
     1 //5X,'MMAX = ',I4,',  NP = ',I2,',  G = ',F4.1
     2 /5X,'DISTRIBUTION : ',3(X,I2),'  (MMIN =',I4,')'
     3 /5X,'DIELECTIC CONSTANTS :  ',F4.1,4(2X,F4.1)
     4 /5X,'A  =',E9.3,',  B  =',E9.3,',  W  =',E9.3,' (M)'
     5 /5X,'D1 =',E9.3,',  D2 =',E9.3,',  D3 =',E9.3,' (M)'
     6 /5X,'SIG3 =',E9.3,',  FREQ = ',F6.2,' (GHZ)' )
C
      IF ( IFLAG2 .EQ. 0 )  GO TO 2010
      WRITE (6,122)  GAM,ATTEN
  122 FORMAT ( /5X,'GAM/KO = ',F9.5,'   ATTEN = ',E11.5,
     1 ' DB/MM' )
      IF ( IFLAG2 .EQ. 1 )  GO TO 2010
      WRITE (6,124)  ZIMP
  124 FORMAT ( /5X,'CHARACTERISTIC IMPEDANCE = ',E11.5,
     1 2X,E11.5 )
 2010 WRITE (6,126)
  126 FORMAT ( /5X,'1  ...   CALCULATE PROPAGATION CONST.'
     1 /5X,'2  ...  CALCULATE PROP. CONST. AND IMPEDANCE'
     2 /5X,'3  ...  CALCULATE CHARACTERISTIC IMPEDANCE'
     3 /5X,'4  ...  CHANGE 1 PARAMETER'
     4 /5X,'5  ...  CHANGE DIMENSIONS, SIG3, AND FREQ'
     5 /5X,'6  ...  CHANGE ALL PARAMETERS'
     6 /5X,'7  ...  CHECK WITH CSVDC'
     7 /5X,'10 ...  GO BACK TO MAIN MENU' )
 2020 READ (5, * )  ICTRL
      IF ( ICTRL.EQ.1 .OR. ICTRL.EQ.2 )  GO TO 2500
      IF ( ICTRL .EQ. 3 )  GO TO 2030
      IF ( ICTRL .EQ. 4 )  GO TO 2400
      IF ( ICTRL .EQ. 5 )  GO TO 2100
      IF ( ICTRL .EQ. 6 )  GO TO 2200
      IF ( ICTRL .EQ. 7 )  GO TO 3500
      IF ( ICTRL .EQ. 10 )  GO TO 1000
      WRITE (6,110)
      GO TO 2020
C
 2030 IF ( IFLAG2 .EQ. 1 )  GO TO 3300
      WRITE (6,110)
      GO TO 2020
C
 2100 WRITE (6,130)
  130 FORMAT ( 5/,5X,'****** INPUT PARAMETERS ******' )
      GO TO 2300
 2200 WRITE (6,130)
      WRITE (6,140)
  140 FORMAT ( /5X,'MMAX, NP, G' )
      READ (5, * )  MMAX,NP,G
      WRITE (6,150)
  150 FORMAT ( /5X,'DIELECTRIC CONSTANTS 1-5' )
      READ (5, * )  EPS1,EPS2,EPS3,EPS4,EPS5
 2300 WRITE (6,160)
```

```
  160 FORMAT ( /5X,'A  B, W (M)' )
      READ (5, * )  A,B,W
      WRITE (6,170)
  170 FORMAT ( /5X,'D1, D2, D3 (M)' )
      READ (5, * )  D1,D2,D3
      WRITE (6,180)
  180 FORMAT ( /5X,'SIG3 (S/M), FREQ (GHZ)' )
      READ (5, * )  SIG3,FREQ
      IFLAG1 = 1
      IFLAG2 = 0
      CALL POINTS (X,NP,J1,J2,J3,Q)
      MMIN = W/(X(J1+2)-X(J1+1))+1
      GO TO 2000
C
 2400 IFLAG2 = 0
      WRITE (6,190)
  190 FORMAT ( /5X,'INPUT NAME OF THE PARAMETER.' )
      READ (5,400)  NAME
  400 FORMAT ( A4 )
      WRITE (6,200)
  200 FORMAT ( /5X,'ITS VALUE' )
      READ (5, * )  VALUE
C
      IF ( NAME .EQ. 4HMMAX )  MMAX = VALUE
      IF ( NAME .EQ. 4HNP   )  GO TO 2410
      IF ( NAME .EQ. 4HQ    )  Q = VALUE
      IF ( NAME .EQ. 4HA    )  A = VALUE
      IF ( NAME .EQ. 4HB    )  B = VALUE
      IF ( NAME .EQ. 4HW    )  W = VALUE
      IF ( NAME .EQ. 4HD1   )  D1 = VALUE
      IF ( NAME .EQ. 4HD2   )  D2 = VALUE
      IF ( NAME .EQ. 4HD3   )  D3 = VALUE
      IF ( NAME .EQ. 4HEPS1 )  EPS1 = VALUE
      IF ( NAME .EQ. 4HEPS2 )  EPS2 = VALUE
      IF ( NAME .EQ. 4HEPS3 )  EPS3 = VALUE
      IF ( NAME .EQ. 4HEPS4 )  EPS4 = VALUE
      IF ( NAME .EQ. 4HEPS5 )  EPS5 = VALUE
      IF ( NAME .EQ. 4HSIG3 )  SIG3 = VALUE
      IF ( NAME .EQ. 4HFREQ )  FREQ = VALUE
      GO TO 2000
 2410 NP = VALUE
      CALL POINTS (X,NP,J1,J2,J3,Q)
      MMIN = W/(X(J1+2)-X(J1+1))+1
      GO TO 2000
C
C        START ROOT SEARCH.
C
 2500 IF ( ICTRL .EQ  1 )  IFLAG2 = 1
      IF ( ICTRL .EQ  2 )  IFLAG2 = 2
      AKO = 20.0*PI*FREQ/2.998
      OMEGA = 2.0E9*PI*FREQ
      ZEPS3 = EPS3 - (0.0,1.0)*SIG3/(OMEGA*ZEP)
C
      DO 5 I=1,NP
      XP(I) = (X(I)+X(I+1))/2.0
    5 CONTINUE
C
      DO 10 N=1,MMAX
      BETA(N) = (FLOAT(N)-0.5)*PI/W
   10 CONTINUE
C
 2700 IFACT = 0
```

```
      IIMP = 0
      NSIG = 4
      ITMAX = 20
      WRITE (6,220)
  220 FORMAT ( /5X,'INPUT INITIAL GUESS:   GAM/KO,  ',
     1 'ATTEN (DB/MM)  ' )
      READ (5, * )  GAM,ATTEN
      CX(1) = GAM*AKO-ZJ*ATTEN/DBN
 2800 WRITE (6,230)
  230 FORMAT ( /5X,'ROOT SEARCH STARTED...'
     1 //5X,'-GAM/KO-',6X,'-ATTEN-',11X,'-DET-',
     2 14X,'-RCOND-' )
C
      CALL ZANLYT (DETERM,0.0,NSIG,0,1,1,CX,ITMAX,INFER,IER)
C
      IF ( REAL(CX(1)) .LT. 0.0 )  CX(1) = -CX(1)
      GAM = REAL(CX(1)) / AKO
      ATTEN = - AIMAG(CX(1))*DBN
C
      IF ( IER .EQ. 0 )  GO TO 3100
      WRITE (6,250)  GAM,ATTEN,IER
  250 FORMAT ( //5X,'****** TERMINAL ERROR (ZANLYT) ******'
     1 /5X,'GAM/KO = ',F9.5,',  ATTEN = ',E11.5,
     2 /5X,' DB/MM,  IER = ',I3
     3 /5X,'1  ...   CONTINUE CALCULATION'
     4 /5X,'2  ...   DIFFERENT INITIAL GUESS'
     5 /5X,'3  ...   CHANGE PARAMETERS' )
 2900 READ (5, * )  ICTRL
      IF ( ICTRL .EQ. 1 )  GO TO 3000
      IF ( ICTRL .EQ. 2 )  GO TO 2700
      IF ( ICTRL .EQ. 3 )  GO TO 2000
      WRITE (6,110)
      GO TO 2900
C
 3000 WRITE (6,260)
  260 FORMAT ( /5X,'ITMAX' )
      READ (5, * )  ITMAX
      GO TO 2800
C
 3100 WRITE (1,500)  MMAX,NP,Q,
     1               EPS1,EPS2,EPS3,EPS4,EPS5,
     2               A,B,W,D1,D2,D3,SIG3,FREQ,
     3               GAM,ATTEN
  500 FORMAT ( 4/,10X,'MMAX = ',I4,',   NP = ',I2,',   Q = ',
     1 F4.1/10X,'DIELECTRIC CONSTANTS :  ',F4.1,4(4X,F4.1)
     2 /10X,'A  =',E9.3,',  B  =',E9.3,',  W  =',E9.3
     3 /10X,'D1 =',E9.3,',  D2 =',E9.3,',  D3 =',E9.3
     4 /10X,'SIG3 =',E9.3,',    FREQ = ',F6.2,' GHZ'
     5 //10X,'GAM/KO = ',F10.6,',    ATTEN = ',E12.6,
     6 ' DB/MM' )
C
      IF ( IFLAG3 .NE. 0 )  GO TO 3300
      IF ( IFLAG2 .EQ. 1 )  GO TO 2000
C
C        CALCULATE IMPEDANCE
C
 3300 IFLAG2 = 2
      IIMP = 1
      CX(2) = DETERM (CX(1))
      PCONST(ISECTN) = CX(1)
      TG(2*(ISECTN-1)+1) = GAM
      TG(2*(ISECTN-1)+2) = ATTEN
```

```
      ZC(ISECTN) = ZIMP
      WRITE (1,510)  ZIMP
  510 FORMAT ( /10X,'CHARACTERISTIC IMPEDANCE = ',
     1 E12.6,2X,E12.6 )
C
      IF ( IFLAG3 .EQ. 1 )  GO TO 4000
      GO TO 2000
C
C        CHECK ACCURACY BY SINGULAR VALUE DECOMPOSITION.
C
 3500 IF ( IFLAG2 .NE. 0 )  GO TO 3510
      WRITE (6,110)
      GO TO 2020
C
 3510 IIMP = 10
      CX(2) = DETERM (CX(1))
      CX(2) = DETERM (CX(1)*(1.0+10.0**(-NSIG)))
      CX(2) = DETERM (CX(1)*(1.0-10.0**(-NSIG)))
      GO TO 2010
C
C        MIS PERIODIC COPLANAR WAVEGUIDE.
C
 4000 WRITE (6,290)  TG(1),TG(2),ZC(1),TG(3),TG(4),ZC(2)
  290 FORMAT ( 5/,5X,'****** PERIODIC STRUCTURE ******'
     1 //5X,'SECTION',5X,'GAM',8X,'ATTEN',14X,'ZC'
     2 /8X,'1',5X,F9.5,2X,E11.5,2X,E9.3,X,E9.3
     3 /8X,'2',5X,F9.5,2X,E11.5,2X,E9.3,X,E9.3 )
      IF ( IFLAG3 .NE. 2 )  GO TO 4010
      WRITE (6,292)  GAM,SHIFT,ATTEN
  292 FORMAT ( /5X,'GAM/KO = ',F9.3,' (',F10.5,')'
     1 /5X,'ATTEN  = ',E11.5 )
 4010 WRITE (6,294)
  294 FORMAT ( /5X,'1  ...  CALCULATION FOR SECTION 1'
     1 /5X,'2  ...  CALCULATION FOR SECTION 2'
     2 /5X,'3  ...  CALCULATE PROPAGATION CONST.'
     3 /5X,'10 ...  GO BACK TO MAIN MENU' )
 4100 READ (5, * )  ICTRL
      IFLAG3 = 1
      IF ( ICTRL .EQ. 1 )  GO TO 4200
      IF ( ICTRL .EQ. 2 )  GO TO 4300
      IF ( ICTRL .EQ. 3 )  GO TO 4500
      IF ( ICTRL .EQ. 10 )  GO TO 4400
      WRITE (6,110)
      GO TO 4100
C
 4200 ISECTN = 1
      GO TO 2000
 4300 ISECTN = 2
      GO TO 2000
 4400 ISECTN = 1
      IFLAG3 = 0
      GO TO 1000
C
 4500 IFLAG3 = 2
      WRITE (6,300)
  300 FORMAT ( //5X,'LENGTH OF EACH SECTION (M)' )
      READ (5, * )  L(1),L(2)
C
      CALL PERIOD (AKC,L,ZC,PCONST,GAM,SHIFT,ATTEN)
C
      WRITE (1,520)  L(1),L(2),GAM,SHIFT,ATTEN
  520 FORMAT ( /10X,'PERIODIC STRUCTURE  ( LENGTHS ',
```

```
     1 E12.6,4X,E12.6/'10X,'GAM/KO = ',F10.6,'   (',
     2 F10.5,'),      ATTEN = ',E12.5 )
      GO TO 4000
      END
C
C
C
C
C
      COMPLEX FUNCTION DETERM (G)
C
C        CONSTRUCTS MATRIX AND CALCULATES ITS DETERMINANT.
C        ALSO SOLVES FOR ELECTRIC FIELD AND CURRENT
C        DENSITY TO CALCULATE CHARACTERISTIC IMPEDANCE.
C
      COMMON    /BLOCK0/A,B,W,D1,D2,D3,AKO,PI,ZMU,ZEP,OMEGA
      COMMON    /BLOCK1/EPS1,EPS2,ZEPS3,EPS4,EPS5
      COMMON    /BLOCK2/BETA(1200)
      COMMON    /BLOCK3/MMAX,NP,J1,J2,J3,IIMP,IFACT,ZIMP
      COMMON    /BLOCK4/X(50),XP(50)
      COMPLEX   G,GAMMA,GAMMA2,ZEPS3,ZIMP,CTAN
      COMPLEX   Z(50,50),WORK(50),SC(50),DET(2)
      COMPLEX   ALPHA(5),O,P,Q,R,S,T,U,V,PCN,PDN,SQBETA
      COMPLEX   P1,Q1,R1,R2,R3,R4,R5,R6,S1,S2
      INTEGER   IPVT(50)
      REAL      EA(50),EP(50)
C
      LDZ = 50
      DBN = 8.6859E-3
      GAMMA = G
      GAMMA2 = GAMMA*GAMMA
      AKO2 = AKO*AKO
C
      DO 10 I=1,NP
      DO 10 J=1,NP
   10 Z(J,I) = (0.0,0.0)
C
      DO 200 N=1,MMAX
      SQBETA = BETA(N)*BETA(N)
      P = GAMMA2 + SQBETA
      ALPHA(1) = CSQRT(P-EPS1*AKO2)
      ALPHA(2) = CSQRT(EPS2*AKO2-P)
      ALPHA(3) = CSQRT(ZEPS3*AKO2-P)
      ALPHA(4) = CSQRT(EPS4*AKO2-P)
      ALPHA(5) = CSQRT(P-EPS5*AKO2)
      O = CTAN(ALPHA(4)*D3)
      P1 = ALPHA(4)/EPS4 + O*ALPHA(5)/EPS5
      Q1 = O*ALPHA(4)/EPS4 - ALPHA(5)/EPS5
      R1 = EPS2/ZEPS3*ALPHA(3)/ALPHA(2)
      R2 = ZEPS3/EPS4*ALPHA(4)/ALPHA(3)
      R3 = CTAN(ALPHA(2)*D1)
      R4 = CTAN(ALPHA(3)*D2)
      R5 = -R1*R3
      R6 = -R2*R4
      S1 = 1.0+Q1/P1*R6
      S2 = R4+Q1/P1*R2
      PCN = -(S1+S2*R5)/(S1*R3+S2*R1)
C
      P1 = ALPHA(4) + O*ALPHA(5)
      Q1 = O*ALPHA(4) - ALPHA(5)
      R1 = ALPHA(3)/ALPHA(2)
      R2 = ALPHA(4)/ALPHA(3)
```

```
      R5 = -R1*R3
      R6 = -R2*R4
      S1 = 1.0+Q1/P1*R6
      S2 = R4+Q1/P1*R2
      PDN = -(S1*R3+S2*R1)/(S1+S2*R5)
C
      T = PDN*ALPHA(2)/ALPHA(1) + 1.0
      S = PCN*EPS2/EPS1*ALPHA(1)/ALPHA(2) + 1.0
      P1 = ALPHA(1)*ALPHA(1)
      V = GAMMA2+S/P1 - T*SQBETA/EPS1/AK02
      P = GAMMA*(T/EPS1/AK02+S/P1)/V
      Q1 = (GAMMA2+SQBETA)/ALPHA(1)/BETA(N)/OMEGA/V
      Q = Q1/EPS1/ZEP
      R = Q1*S*T/ZMU
C
      I1 = J1+1
      I2 = J1+J2
      I3 = J1+J2+1
C
      DO 600 I=1,J1
  600 SC(I) = COS(BETA(N)*XP(I))
      DO 610 I=I1,I2
  610 SC(I) = SIN(BETA(N)*XP(I))
      DO 620 I=I3,NP
  620 SC(I) = COS(BETA(N)*XP(I))
C
      XSCJ = 0.0
      DO 50 J=1,J1
      XSCJ1 = SIN(BETA(N)*X(J+1))
      XT = XSCJ1 - XSCJ
      XSCJ = XSCJ1
      DO 20 I=1,J1
      Z(I,J) = Z(I,J)-Q*XT*SC(I)
   20 CONTINUE
      DO 30 I=I1,I2
      Z(I,J) = Z(I,J)+P*XT*SC(I)
   30 CONTINUE
      DO 40 I=I3,NP
      Z(I,J) = Z(I,J)+Q*XT*SC(I)
   40 CONTINUE
   50 CONTINUE
C
      XSCJ = COS(BETA(N)*X(I1))
      DO 90 J=I1,I2
      XSCJ1 = COS(BETA(N)*X(J+1))
      XT = XSCJ1 - XSCJ
      XSCJ = XSCJ1
      DO 60 I=1,J1
      Z(I,J) = Z(I,J)-R*XT*SC(I)
   60 CONTINUE
      DO 70 I=I1,I2
      Z(I,J) = Z(I,J)-R*XT*SC(I)
   70 CONTINUE
      DO 80 I=I3,NP
      Z(I,J) = Z(I,J)-R*XT*SC(I)
   80 CONTINUE
   90 CONTINUE
C
      XSCJ = SIN(BETA(N)*X(I3))
      DO 130 J=I3,NP
      XSCJ1 = SIN(BETA(N)*X(J+1))
      XT = XSCJ1 - XSCJ
```

```
      XSCJ = XSCJ1
      DO 100 I=1,J1
      Z(I,J) = Z(I,J)+G*XT*SC(I)
  100 CONTINUE
      DO 110 I=I1,I2
      Z(I,J) = Z(I,J)-F*XT*SC(I)
  110 CONTINUE
      DO 120 I=I3,NP
      Z(I,J) = Z(I,J)+G*XT*SC(I)
  120 CONTINUE
  130 CONTINUE
  200 CONTINUE
C
      IF ( IIMP .EQ. 10 )  GO TO 700
      CALL CGECO (Z,LDZ,NP,IPVT,RCOND,WORK)
      IF ( IIMP .EQ. 1 )  GO TO 400
      CALL CGEDI (Z,LDZ,NP,IPVT,DET,WORK,10)
      IF ( IFACT .NE. 0 )  GO TO 325
      FACTOR = REAL(DET(2))
      IFACT = 10
  325 DETERM = DET(1) * 10.0**(REAL(DET(2))-FACTOR)
      GAM = REAL(GAMMA)/AKO
      ATT = -AIMAG(GAMMA)*DBN
      EDET = REAL(DET(2))
      WRITE (6,330)  GAM , ATT , DET(1) , EDET , RCOND
  330 FORMAT ( 1H ,4X,F8.4,2X,E11.4,3X,F7.4,1X,F7.4,1X,*E*,
     1 F5.0,2X,E10.3 )
      RETURN
C
  400 CALL CGESL (Z,LDZ,NP,IPVT,WORK,0)
      P = (0.0,0.0)
      G = (0.0,0.0)
      DO 500 I=1,J1
      P = P-WORK(I)*(X(I+1)-X(I))
  500 CONTINUE
      DO 510 I=I1,I2
      G = G+WORK(I)*(X(I+1)-X(I))
  510 CONTINUE
      WRITE (1,450)
  450 FORMAT ( /// )
      DO 520 I=1,NP
      WORK(I) = WORK(I)/G
      FLDR = REAL(WORK(I))
      FLDI = AIMAG(WORK(I))
     FLDA = CABS(WORK(I))
      FLDP = PHASE(WORK(I))
      WRITE (1,470)  XP(I),FLDR,FLDI,FLDA,FLDP
  470 FORMAT ( 5X,'X =',E9.3,3X,'(REAL)',E13.7,5X,
     1 '(IMAGINARY)',E13.7,5X,'(ABSOLUTE)',E13.7,
     2 5X,'(PHASE)',F7.2 )
  520 CONTINUE
      ZIMP = G/P/2.0
      RETURN
C
  700 LDU = 1
      LDV = 1
      JOB = 0
C
      CALL CSVDC (Z,LDZ,NP,NP,SC,EA,U,LDU,V,LDV,
     1                 WORK,JOB,INFO)
      RCOND = REAL(SC(NP)/SC(1))
      GAM = REAL(GAMMA)/AKO
```

```
      ATT = -AIMAG(GAMMA)*DBN
C
      WRITE (6,710)  GAM,ATT,RCOND,INFO
  710 FORMAT ( 1H ,5X, 'GAM=',F8.4,3X,'ATT=',E12.6,3X,
     1 'RCOND=',E10.4,3X,'INFO=',I2 )
      RETURN
      END
C
C
C
C
C
      SUBROUTINE POINTS (X,NP,J1,J2,J3,Q)
C
C        GENERATES NON-UNIFORM DISTRIBUTION OF THE
C        MATCHING POINTS.
C
      COMMON     /BLOCK0/A,B,W,D1,D2,D3,AKO,PI,ZMU,ZEP,OMEGA
      DIMENSION X(101)
C
      Y0 = EXP(-Q)
      Y1 = EXP(Q*(A-B)/A/2.0)
      Y2 = EXP(Q*(B-W)/A)
      YT = 4.0-Y0-2.0*Y1-Y2
      I1 = INT(FLOAT(NP)*(1.0-Y0)/YT+0.5)
      I2 = INT(FLOAT(NP)*(1.0-Y1)/YT+0.5)
      I3 = NP-I1-2*I2
C
      X(1) = 0.0
      DO 10 I=2,I1
      X(I) = ALOG(FLOAT(I-1)*(1.0-Y0)/FLOAT(I1)+Y0)*A/Q + A
   10 CONTINUE
      X(I1+1) = A
      DO 20 I=2,I2
      X(I1+I) = -ALOG(1.0-FLOAT(I-1)*(1.0-Y1)/FLOAT(I2))*A/Q + A
   20 CONTINUE
      X(I1+I2+1) = (A-B)/2.0
      DO 30 I=2,I2
      X(I1+I2+I) = ALOG(FLOAT(I-1)*(1.0-Y1)/FLOAT(I2)+Y1)
     1            *A/Q + B
   30 CONTINUE
      X(I1+2*I2+1) = B
      DO 40 I=2,I3
      X(I1+2*I2+I) = -ALOG(1.0-FLOAT(I-1)*(1.0-Y2)
     1               /FLOAT(I3))*A/Q + B
   40 CONTINUE
      X(NP+1) = W
      J1 = I1
      J2 = 2*I2
      J3 = I3
      RETURN
      END
C
C
C
C
C
      SUBROUTINE PERIOD (AKO,L,ZC,PR,GAM,SHIFT,ATTEN)
C
C        CALCULATES COMPLEX PROPAGATION CONSTANTS
C        OF THE PERIODIC STRUCTURE.
C
```

```
C
C       -------*************-------------*******
C          . .        -1-            -2-        . .
C       -------*************-------------*******
C              <--- L1 ---> <--- L2 --->
C
      COMPLEX     ZC(2),ZK,PR(2),GAMMA,Z
      REAL        L(2),L1,L2,BETA(2),ATT(2)
C
      DBN = 8.6859E-3
      L1 = L(1)
      L2 = L(2)
      ZK = ZC(1)/ZC(2)
C
      Z = ((ZK+1.0)**2*CCOS(PR(1)*L1+PR(2)*L2)
     1   -(ZK-1.0)**2*CCOS(PR(1)*L1-PR(2)*L2))/4.0/ZK
      GAMMA = CLOG(Z+CSQRT(Z*Z-1))/(L1+L2)
      SHIFT = 6.283185307179/(L1+L2)/AKO
      IF ( AIMAG(GAMMA) .LT. 0.0 )  GAMMA = -GAMMA
      GAM = AIMAG(GAMMA)/AKO
      ATTEN = REAL(GAMMA)*DBN
      RETURN
      END
C
C
C -- END OF THE PROGRAM --
C
```

REFERENCES

1. H. Guckel, P. A. Brennan, and I. Palócz, "A Parallel-Plate Waveguide Approach to Microminiaturized, Planar Transmission Lines for Integrated Circuits," IEEE Trans. Microwave Theory Tech., vol.MTT-15, no.8, pp.468-476, August 1967.
2. H. Hasegawa, M. Furukawa, and H. Yanai, "Properties of Microstrip Line on Si-SiO_2 System," IEEE Trans. Microwave Theory Tech., vol.MTT-19, no.11, pp.869-881, November 1971.
3. G. W. Hughes and R. M. White, "Microwave Properties of Nonlinear MIS and Schottky-Barrier Microstrip," IEEE Trans. Electron Devices, vol.ED-22, no.10, pp.945-956, October 1975.
4. J. M. Jaffe, "A High-Frequency Variable Delay Line," IEEE Trans. Electron Devices, vol.ED-19, no.12, pp.1292-1294, December 1972.
5. D. Jäger, W. Rabus, and W. Eickhoff, "Bias-Dependent Small-Signal Parameters of Schottky Contact Microstrip Lines," Solid-State Electron., vol.17, no.8, pp.777-783, August 1974.
7. E. M. Bastida and G. P. Donzelli, "Periodic Slow-Wave Low-Loss Structures for Monolithic GaAs Microwave Integrated Circuits," Electron. Lett., vol.15, no.19, pp.581-582, September 1979.
8. S. Seki and H. Hasegawa, "Cross-Tie Slow-Wave Coplanar Waveguide on Semi-Insulating GaAs Substrates," Electron. Lett., Vol.17, no.25, pp.940-941, December 1981.

9. P. Kennis and L. Faucon, "Rigorous Analysis of Planar MIS Transmission Lines," Electron Lett., vol.17, no.13, pp.454-456, June 1981.

10. H. Hasegawa and H. Okizaki, "M.I.S. and Schottky Slow-Wave Coplanar Striplines on GaAs Substrates," Electron. Lett., vol.13, no.22, pp.663-664, October 1977.

11. M. Aubourg, J.-P. Villotte, F. Godon, and Y. Garault, "Finite Element Analysis of Lossy Waveguides - Application to Microstrip Lines on Semiconductor Substrate," IEEE Trans. Microwave Theory Tech., vol.MTT-31, no.4, pp.326-331, April 1983.

12. Y.-C. Shih and T. Itoh, "Analysis of Printed Transmission Lines for Monolithic Integrated Circuits," Electron. Lett., vol.18, no.14, pp.585-586, July 1982.

13. Y. Fukuoka and T. Itoh, "Analysis of Slow-Wave Phenomena in Coplanar WAveguide on a Semiconductor Substrate," Electron. Lett., vol.18, no.14, pp.589-590, July 1982.

14. R. Sorrentino and G. Leuzzi, "Full-Wave Analysis of Integrated Transmission Lines on Layered Lossy Media," Electron. Lett., vol.18, no.14, pp.607-609, July 1982.

15. Y. Fukuoka, Y.-C. Shih, and T. Itoh, "Analysis of Slow-Wave Coplanar Waveguide for Monolithic Integrated Circuits," IEEE Trans. Microwave Theory Tech., vol.MTT-31, no.7, pp.567-573, July 1983.

16. E. Yamashita and K. Atsuki, "Analysis of Microstrip-Like Transmission Lines by Nonuniform Discretization of Integral Equations," IEEE Trans. Microwave Theory Tech., vol.MTT-24, no.4, pp.195-200, April 1976.

17. R. F. Harrinton, Time-Harmonic Electromagnetic Fields, New York: McGraw-Hill, 1961.

18. C. P. Wen, "Coplanar Waveguide: A Surface Strip Transmission Line Suitable for Nonreciprocal Gyromagnetic Device Applications," IEEE Trans. Microwave Theory Tech., vol.MTT-17, no.12, pp.1087-1090, December 1969.

19. R. E. Collin, Field Theory of Guided Waves, New York: McGraw-Hill, 1960.

20. D. G. Fink and A. A. McKenzie, Electronics Engineers' Handbook, New York: McGraw-Hill, 1975.

END

FILMED

10-84

DTIC